

Article

Morphology of Dome- and Tepee-like Landforms Generated by Expansive Hydration of Weathering Anhydrite: A Case Study at Dingwall, Nova Scotia, Canada

Adrian Jarzyna ^{1,*} , Maciej Babel ^{1,*}, Damian Ługowski ¹ and Firouz Vladi ²

¹ Faculty of Geology, University of Warsaw, ul. Żwirki i Wigury 93, PL-02-089 Warsaw, Poland; lugowski.damian@gmail.com

² Deutsches Gipsmuseum und Karstwanderweg e.V., Duna 9a, D-37520 Osterode, Germany; fvladi@t-online.de

* Correspondence: a.jarzyna@student.uw.edu.pl (A.J.); m.babel@uw.edu.pl (M.B.)

Abstract: The gypsum-anhydrite rocks in the abandoned quarry at Dingwall (Nova Scotia, Canada) are subjected to physical and chemical weathering, including hydration of the anhydrite, i.e., its transformation into secondary gypsum under the influence of water. This process is known to lead to the localized volume increase of the rock and the formation of spectacular hydration landforms: domes, tepees and ridges. Cavities appearing in the interior of these domes are often unique hydration caves (*Quellungshöhlen* in German). For the first time, this paper gives detailed geomorphometric characteristics of the 77 dome- and tepee-like hydration landforms growing today at Dingwall based on their digital surface models and orthophotomaps, made with the method of photogrammetry integrated with direct measurements. The length of hydration landforms varies from 1.86 to 23.05 m and the relative height varies from 0.33 to 2.09 m. Their approximate shape in a plan view varies from nearly circular, through oval, to elongated with a length-to-width ratio rarely exceeding 5:2. Length, width and relative height are characterized by moderate mutual correlation with proportional relations expressed by linear equations, testifying that the hydration landforms generally preserve the same or very similar shape independent of their sizes. The averaged thickness of the detached rock layer ranges from 6 to 46 cm. The size of the forms seems to depend on this thickness—the forms larger in extent (longer) generally have a thicker detached rock layer. Master (and other) joints and, to a lesser extent, layering in the bedrock influence the development of hydration landforms, particularly by controlling the place where the entrances are open to internal cavities or caves. Three structural types of the bedrock influencing the growth of hydration forms were recognized: with master joints, with layering and with both of them. The latter type of bedrock has the most complex impact on the morphology of hydration landforms because it depends on the number of master joint sets and the mutual orientation of joints and layering, which are changeable across the quarry. The durability of the hydration forms over time depends, among others, on the density of fractures in the detached rock layer.

Keywords: anhydrite; gypsum; hydration landforms; weathering; photogrammetry; geomorphometric analysis; structural analysis



Citation: Jarzyna, A.; Babel, M.; Ługowski, D.; Vladi, F. Morphology of Dome- and Tepee-like Landforms Generated by Expansive Hydration of Weathering Anhydrite: A Case Study at Dingwall, Nova Scotia, Canada. *Appl. Sci.* **2022**, *12*, 7374. <https://doi.org/10.3390/app12157374>

Academic Editors: Giovanni Randazzo, Anselme Muzirafuti and Stefania Lanza

Received: 9 May 2022

Accepted: 14 July 2022

Published: 22 July 2022

Publisher's Note: MDPI stays neutral with regard to jurisdictional claims in published maps and institutional affiliations.



Copyright: © 2022 by the authors. Licensee MDPI, Basel, Switzerland. This article is an open access article distributed under the terms and conditions of the Creative Commons Attribution (CC BY) license (<https://creativecommons.org/licenses/by/4.0/>).

1. Introduction

The hydration forms of relief described in this paper are rare morphological forms appearing in the weathering zone of gypsum-anhydrite rocks [1–9]. They are more or less convex in shape and reach up to 2–3 m in height and over several meters in lateral extension. Their origin is related to the phenomenon of volume increase during hydration of exposed anhydrite rocks under the influence of surface and subsurface waters [10–12] (and further references in [13,14]). During this process, which can be called expansive gypsification of anhydrite [14], the anhydrous calcium sulfate (the mineral anhydrite; CaSO_4) transforms into calcium sulfate dihydrate ($\text{CaSO}_4 \cdot 2\text{H}_2\text{O}$; gypsum) according to the

reaction: $\text{CaSO}_4 + 2\text{H}_2\text{O} \rightarrow \text{CaSO}_4 \cdot 2\text{H}_2\text{O}$. This reaction can lead to volume increase only if the system is open, i.e., when the water is added from the outside [11].

The term hydration form was first used by Hunt et al. [3] (p. 6) for characteristic small-scale forms of relief “unique to karst developed on anhydrite” when “anhydrite hydrates and is changed into gypsum” and “experiences a 1.557 times increase in volume.” They described hydration polygons, domes and crusts in Tripolitania province in Libya. Earlier, hydration domes with internal hydration caves were recognized in the Harz Mts. region in Germany [15].

The majority of the known hydration forms are created as a result of the localized hydration of the anhydrite substrate, leading to volume expansion and local uplift of the surface layer of the rock split of the substrate. These forms commonly show a narrow empty fissure or cavity inside [6,16–18], rarely are they massive [3,19]. Some empty cavities reach sizes large enough to be called caves. They are up to 1.5 [5,7] or even 2.3–2.4 m high [4,20], providing the possibility for an adult man to enter inside. The name hydration caves or swelling caves (*Quellungshölen* in German) was proposed for them [15,21–24]. Caves of this type are very rare in the world [25–27].

The convex hydration forms of the relief were apparently created by expansion of the rock material taking place locally, very close to the surface. According to Breisch and Wefer [17], the shape of the forms is generally a product of eccentrically acting compressive stress within the localized hydration zone. The differential expansion greater at the surface than in the rock interior causes detachment of the surface layer of the rock and its uplift, leading to empty dome- or tepee-like hydration forms, including pressure ridges. The volume expansion of the rock material is led by displacive crystallization of secondary gypsum, exerting crystallization pressure on the surroundings [14]. It has been recognized that these processes and expansions leading to the growth of the forms take place not only within the uplifted layer but also in the nearest vicinity of the forms [4,28].

The hydration forms of relief have a specified origin, shapes and sizes, and occur as discrete objects on the Earth’s surface. Thus, they show the basic features defining landforms [29–31], and as such, they can be a subject of geomorphometric analysis [30,32–35].

Hydration landforms may occur in groups, creating a rare type of morphology, which can be called a hydration landscape. The discussed forms (as well as the similar weathering forms of the relief—gypsum tumuli [36,37])—can be considered a unique type of landform characteristic of sulfate karst [38] (pp. 125–126), yet not satisfactorily recognized and known.

Occurrences of hydration forms and caves have been documented in many places around the world, both in natural (e.g., Woodward Co. in Oklahoma, Ottawa Co. in Ohio, Culberson Co. in Texas, and Eddy Co. in New Mexico in the USA, Alberta in Canada, and Tripolitania in Libya) and artificial exposures of anhydrite rocks [3,4,15–17,19,22,39–50]. However, so far, only four places are known with remarkable amounts of these forms creating spectacular hydration landscape: most notably at environs of Walkenried at the south margin of Harz Mts. in Germany [2,4,6,15,47,49,51–53], in the abandoned quarry at Pisky in Ukraine [13,18,54–60], on the small Alebastrovyye Islands in Russia [5] and at the abandoned quarry at Dingwall in Canada [6–9,14,48,61]. Among them, the site at Dingwall in Canada (Figures 1 and 2a–e), studied by the authors, is the largest in number and size of hydration forms and caves. This permits the investigation of their geomorphometric features in a statistical way.

During the growth of these landforms, the rock creates a generally convex shape, described as dome-like, but also tepee-like, triangular in cross-section (tents in [48]) [6,61]. The other authors called them gypsum bubbles due to their predominantly dome-like shape [6,17,39,48], mounds [5,16], and blisters [42,48], but because of their similarity to the characteristic low wall-less army tents—also tents or A-tents [48,62]. Based on the observation of changes in the form shape over time (Figure 2e,f) [7,9], it has been proposed that the shape of the forms from Dingwall will change from a dome (bubble) to a tepee (tent [48]), similar to the case of the hydration form called Waldschmiede in Germany [4,49].

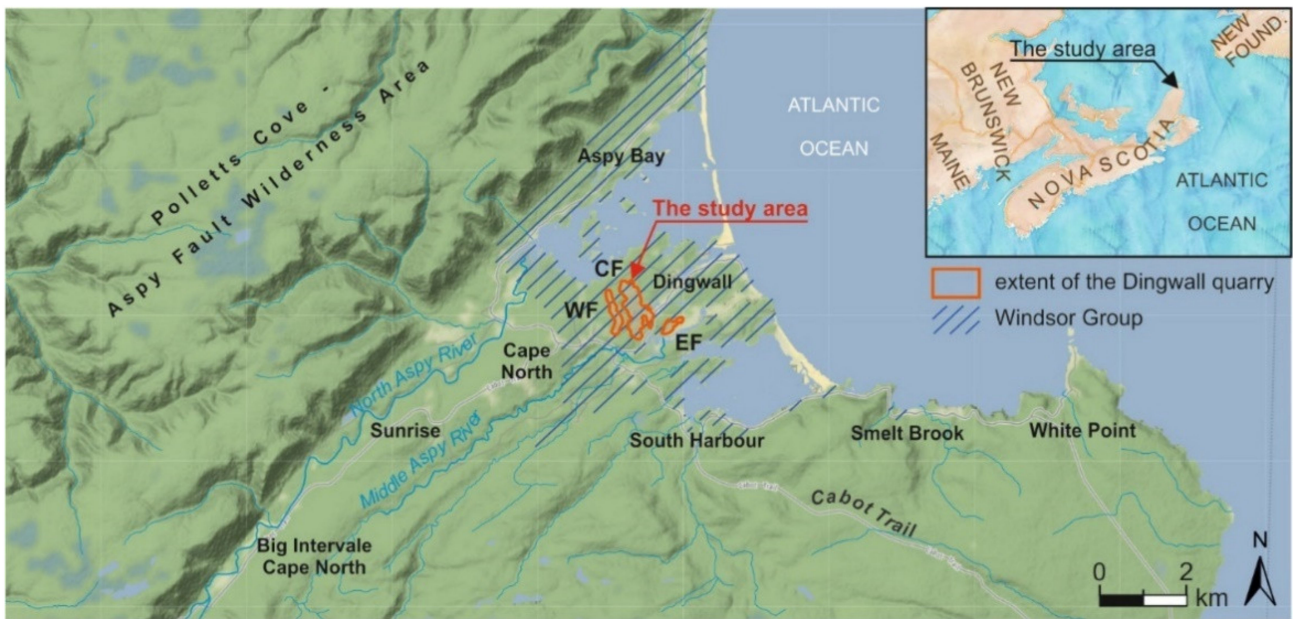


Figure 1. Location of the abandoned gypsum quarry at Dingwall, eastern Canada, along with Windsor Group. Quarry is divided into the western field (WF), the central field (CF) and the eastern field (EF). Source of maps: ArcGIS program (Esri, Redlands, CA, USA) and <http://maps.stamen.com> (accessed on 25 June 2022).



Figure 2. Cont.

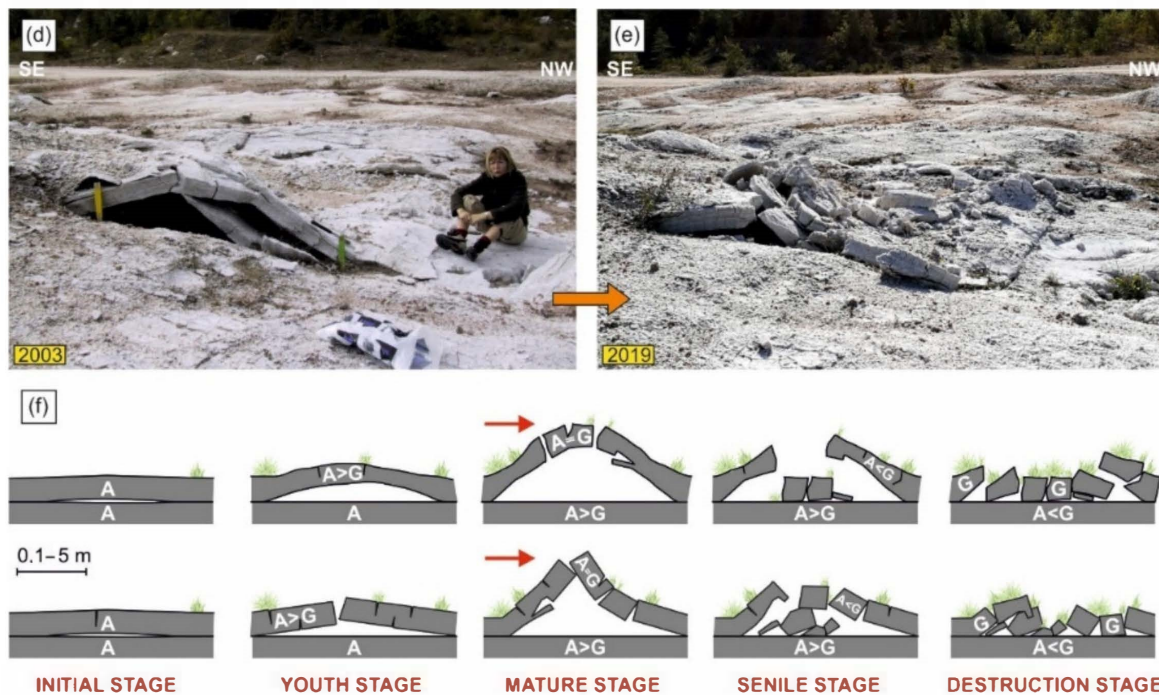


Figure 2. Hydration landscape and landforms at Dingwall in photographs taken with the use of UAV (a–c) and digital camera (d,e) and interpretation of their development (f); (a) northern part of the CF (Figure 1); (b) view of the CF showing form no. 15 with hydration cave named Personal Grotto (see Section 4.1) with the author (D.L.), (a) and (b) photographs were taken on 28 August 2019; (c) the largest hydration cave, Ramesh Cave seen from above (the authors F.V., A.J., D.L. are on the photograph taken on 21 September 2018); (d,e) sixteen-year morphological evolution of exemplary hydration dome from mature to destruction stage; note the development of weathering debris from massive anhydrite bedrock, such as one on which Susanne Vladi is sitting; form without identification number located 10 m east of the Ramesh Cave (see Section 4.1); (f)—evolution stages of domed (upper row) and tepee-like (lower row) anhydrite hydration form associated with changes in mineralogical composition (A—anhydrite, G—gypsum); maximum relative height is indicated by red arrow [57].

An intermediate form similar to both was called the rounded tent [48]. Deformations formed during gypsification can also take a more diverse, irregular and difficult to define shape, such as a bridge [18], or elongated forms, such as long ridges, called pressure ridges [7].

The studied tepee-like hydration landforms represent the morphological equivalent of the well-known tepee structures commonly recorded in carbonate and evaporite rocks [63] but differ from them in not forming polygonal ridges but creating isolated forms rounded in a plan view. Only the elongated hydration pressure ridges co-occurring with the studied forms are equivalents of the typical tepee structures. Many tepee-like hydration landforms are similar to granite A-tents or “pop-ups” landforms [62,64–66]. On the other hand, the dome-like hydration forms are very similar to those of the gypsum tumuli [36,37,67].

Hydration forms usually develop on the anhydrite-dominated bedrock, characterized by varying degrees of coverage by fractures but also with massive structures [4,5,14]. The fractures are not only the migration path of the fluids, causing the transition of anhydrite to gypsum and generating the development of forms. They also influence the shape and orientation of the growing forms. Stenson [48] found at Dingwall that when fractures are present in the bedrock, “tents” with sharp crests and triangular vertical cross-sections develop, while in the absence of them, the rock deforms in a more “plastic” way, generating more rounded forms, such as bubbles or blisters. Near Walkenried, the dependence of the position and elongation of hydration domes and the accompanying depressions on

the system of joints have been documented by Reimann [4]. In turn, the elongation of hydration forms from the Alebastrovyie Islands was found to be generally parallel to the strike of the anhydrite layers [5].

Lateral sizes of the discussed forms reach values of more than 10 m (Table 1) [2,5,8,18], in extreme cases of pressure ridges, even 25 m [61]. The largest documented hydration landform was the Great Dome at Pisky, which has dimensions of 18.1 × 15.5 × 3.0 m, with an inner cave of 9.5 × 7.8 × 1.2 m [18,58]. The other large hydration form found in the forest near Walkenried was Waldschmiede (Forest Forge). Its dimensions in 1933 were 10.0 × 7.0 × 1.9 m [68] and its inner cave measured a few years earlier was 8.0 × 7.5 × 2.0 m in size [53]. The height of this growing cave was 2.3 m, although their lateral sizes shrunk [1,4,58]. Another hydration form of extraordinary size is the Ramesh Cave in the Dingwall quarry, with dimensions of 9.95 × 4.10 × 1.32 m [8]. Documented sizes of hydration caves are often changeable and grow or decrease with time [4,9,49]. A detached rock layer is commonly from a few cm to several tens of cm thick [5,6,18,51,53,61], and in extreme cases, in side parts of forms 200 cm thick [9]. The thicker layers, as a rule, occur above the largest hydration caves [45].

Table 1. Morphometric data of anhydrite hydration landforms (including pressure ridges at Dingwall) and hydration caves at Pisky, Walkenried, the Alebastrovyie Islands and Dingwall.

Site Name/ Province/ Country	Pisky/ Lviv Oblast/ Ukraine	Walkeried/ Lower Saxony/ Germany	Alebastrovyie Islands/ Novaya Zemlya/Russia	Dingwall/ Nova Scotia/ Canada
References	[7,13,18,20,28,54–60]	[1,2,4,6,7,49,51,68]	[5]	[6–9,14,48,61]
Number of documented hydration forms	99	26	unknown number	69 *
Area with hydration relief	200 × 300 m	1300 × 600 m	800 × 150 m	1800 × 1400 m
Range of dimensions of hydration forms	length: 0.58–18.1 m width: 0.32–15.5 m height: 0.05–3.0 m	length: <10 m width: 7.0 m height: <3 m	length: 3–15 m width: 1–10 m height: 0.5–1.5 m	length: <25 m width: 0.8–8.2 m height: 0.1–2.4 m
Range of dimensions of inner hydration caves	length: <9.5 m. width: <7.8 m height: <2.4 m	length: <10 m width: <7.5 m height: <2.3 m	length: unknown width: unknown height: <1.5 m	length: <10.7 m width: <6.6 m height: <1.32 m

*—data after Stenson [48].

Until now, the most frequently used methods in the study of hydration forms were standard geological and geomorphological observations, drawing and photographing. Measurements of the most important dimensions, such as length, width and height, were made with a ruler, but also a laser rangefinder. Moreover, the azimuth of elongation was measured with a geological compass and location was noted by a GPS device [18,48]. Terrestrial photogrammetry was recently used at Pisky, which, in combination with ArcGIS (Esri, Redlands, CA, USA) and Photoscan (Agisoft LLC, St. Petersburg, Russia) computer programs, was the basis for supplementary morphometric measurements [57,60]. To measure the change in the distance between the two points in time, the benchmark method with metal bolts was used [6,60]. At Dingwall, Stenson [48] applied statistical analysis of measured geomorphometric parameters of 69 hydration landforms (Table 1), calculating, inter alia, the average or the minimum and maximum value, and also calculated unknown parameters on the basis of already determined dimensions. However, Dingwall does not yet have detailed and comprehensive documentation of aerial and terrestrial photogrammetry and geomorphometric analysis based on these data.

Morphometric three-dimensional features, sizes and spacings are crucial for characterizing any landform [29] and also for remote recognition of them both on Earth and the other planets [30,69]. Hydration forms of relief analogous to terrestrial ones can potentially be present on Mars [70].

The aim of this paper is to give the geomorphometric characteristics of the anhydrite hydration landforms from Dingwall. The shapes, sizes and other distinctive morphological features of these poorly known forms are described quantitatively with the use of photogrammetric and statistical methods of analysis for the first time. Our study is based on the examination of a relatively large number of forms and supplements to previous information on this subject. We also attempted to recognize the influence of the structural elements of the weathering anhydrite bedrocks, such as joints and layering, on the morphology of the hydration forms and their evolution. The hydration forms from Dingwall are compared with similar hydration forms and other landforms found elsewhere on the substrate of weathering anhydrite and gypsum rocks.

2. Study Area

The studied quarry is located on the north side of Cape Breton Island in Victoria Co., on the edge of both Dingwall and Cape North villages (Figure 1). The mining of gypsum in the excavation was carried out by the National Gypsum Company in 1933–1955 [71,72].

The bedrock of the study area consists of Precambrian igneous-metamorphic rocks intruded by Devonian magmatic bodies with a predominantly granite composition [71,73]. The bedrock is covered with the Carboniferous evaporitic-clastic deposits [71], which include the Horton Group (Tournaisian) [74] and the Windsor Group (Visean) [71], the latter exposed at Dingwall quarry (Figure 1). The next younger rocks are Quaternary in age and are related to the activity of the Wisconsinan ice sheet, lasting from 75 or 65 to 11–10 ka [75,76]. It left the layers of tills lying on the eroded Carboniferous and older rocks.

The gypsum-anhydrite layers in the studied quarry show a variable arrangement. The data collected in the field and from the available maps [71] indicate that the predominant dip is in the eastern direction and its value mostly oscillates between 15° and 30°, but also is horizontal (see Section 4.6.3) [14].

The outcrop is characterized by several meters deep, vertically elongated and narrow in shape Schlottenkarren (densely packed, funnel-shaped sinkholes draining into vertical cylindrical shafts [76,77]). According to Moseley [76], they can be either exhumed forms originating before the ice sheet comes or post-glacial in age. Currently, the Dingwall area is subjected to intensive karst solution, including the formation of gypsum karren [48,78].

The climate of Dingwall is temperate and cold [14]. According to ClimateCharts.net [79,80] in the quarry area (34 m a.s.l., based on data from 1901–2019), the precipitation reaches 1242.7 mm/year with monthly values between 85.8 mm (in July) and 136.6 mm (in November). The mean temperature is 4.7 °C. The coldest month is February, with an average temperature of −6.7 °C, and the warmest one is August, with an average temperature of 16.4 °C.

3. Materials and Methods

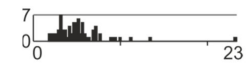
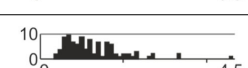
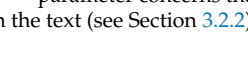
3.1. Field and Laboratory Photogrammetric Works

Fieldworks were led during two expeditions in 2018 (10–26 September) and 2019 (15–29 August). We measured all the largest dome- and tepee-like hydration forms with internal caves and the largest hydration chambers using a laser range finder and tape measure. Smaller hydration domes and tepee-shaped forms of a few to several tens of centimeters in height and less than ca. 1.8 m in diameter in a plan view are very abundant at the site (e.g., see Section 4.1) (Figure 7 in [9]). These as well as badly damaged forms (Figure 2d,e) and some pressure ridges up to 1 m or more in height were omitted from our quantitative documentation. We also did not measure irregular detachments of the rock layers (see Section 4.1) and extensive, almost flat uplifts of these layers, with an extension of several meters or more.

Our investigations focused on convex hydration landforms showing significant sizes—those that attain more than about 2 m in diameter. The basic identification criteria used for their recognition were as follows: (1) pronounced convex shape, (2) the presence of a cavity under the rock surface; when this cavity was invisible, then its presence was detected by the rumble sound during hitting the ground with a hammer.

The hydration forms were recorded by direct measurements and photogrammetric methods using Unmanned Aerial Vehicle (UAV) and digital cameras. Photogrammetry was also used to visualize the bottom of the quarry and the individual forms. During field work, the form was identified with the assignment of a documentation number, its most important morphometric parameters (Table 2; Figure 3) and the location. The delimitation of the forms in the plan view was outlined on the basemap of the orthophotomap with the use of a portable mobile device (Lenovo Yoga Tab 3, Hong Kong, China). Joints and fractures were measured with a geological compass and distances with the laser rangefinder and the tape measure.

Table 2. Geomorphometric parameters measured and computed for 74 hydration forms, including symbol, unit, formula, maximum, minimum and average value, references and frequency distribution diagrams (horizontal axis has the same unit as the parameter, vertical axis is the number of measurements).

Name of Parameter	Symbol, Unit and Formula (If Applied)	Maximum–Minimum; Average Value	Number of Measurements	References	Simplified Frequency Distribution Diagrams
Length *	a (m)	1.86–23.05; <u>5.25</u>	74	[36] modified; [67] modified; [81] modified; [82,83]	
Width	b (m)	0.92–9.01; <u>8.38</u>	74	[36] modified; [67] modified; [81] modified; [82,83]	
Relative height	h_r (m)	0.33–2.09; <u>0.83</u>	74	[84] modified	
Thickness of detached layer	e (m)	0.06–0.46; <u>0.21</u>	54	[18,36,64]	
Coefficient of circularity	$C (-) (a - b)/a$	0.04–0.73; <u>0.33</u>	74	[18,36,67]	
Azimuth of elongation orientation	Az (°)	0–176 ****; <u>84</u>	68	New	
Bulge degree	$B (-) b/h_r$	1.82–8.58; <u>4.28</u>	74	[84]	
Fracture density	$F_D (m/m^2) \sum L_s/P$ ***	0.04–3.38; <u>0.85</u>	69	[85,86] modified	
Length of the entrance line **	— (m)	0.30–4.52; <u>1.21</u>	98	New	
Azimuth of the entrance line **	— (°)	0–177 ****; <u>92</u>	98	New	
Azimuth of entrance **	— (°)	0–350 ****; <u>92</u>	92	[18]	
Direction of maximum lateral expansion	— (°)	3–67, 80–115, 130–176 ****; <u>83</u>	66	[66] modified	

*—measurements do not involve small hydration forms with a length less than 1.8 m, **—parameter concerns the entrance to hydration cavity or cave inside the form, ***—explanations of symbols in the text (see Section 3.2.2), ****—range of the values.

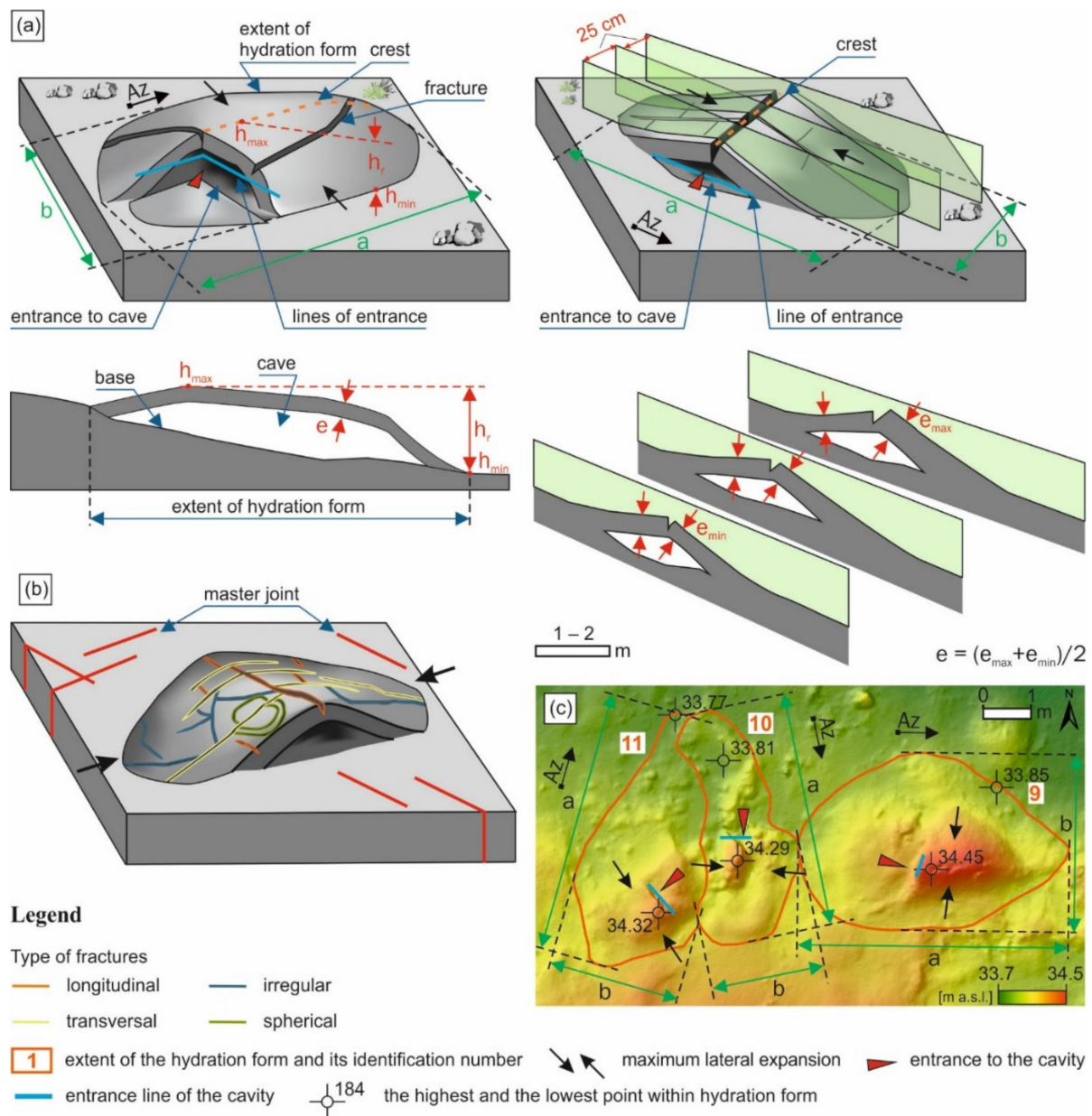


Figure 3. Morphometric parameters of domed (top left) and tepee-like hydration forms (top right) with method of measuring and calculation of the thickness of detached rock layer using cross sections through *.las* data, presented both on schematic drawings (a) and exemplary DMSs (c), and types of fractures recorded within hydration landforms including those inherited from master joints (b); a—length of the form in plan view; b—width of the form in plan view; Az—azimuth of elongation orientation; e—thickness of detached rock layer; e_{min} —the smallest, measured thickness; e_{max} —the largest, measured thickness; h_r —relative height; h_{max} —the largest value of elevation within extent of the form; h_{min} —the smallest value of elevation within extent of the form. Further explanations in the text.

The applied methodology of photogrammetric documentation is described in the previous work of the authors [7], the other papers [87–89], the instructions for the program used [90] and in the supplementary materials (Figure S1). These works mainly involved the use of the Photoscan program (Agisoft LLC, St. Petersburg, Russia) based on the Structure-From-Motion method [89]. The usefulness and effectiveness of the applied photogrammetric methodology in geospatial analysis have been demonstrated in many papers (e.g., [91]).

3.2. Methodology of Dataset Analysis

3.2.1. Analysis of Morphology and Morphometry

An orthophotomap and a Digital Surface Model (DSM) were created for every studied hydration landform involving its surroundings. The forms are most commonly domed (e.g., Figure 2b) or tepee-like in shape (e.g., Figure 2c). The basis for distinguishing the tepee-shaped forms is the presence of at least two rock slabs with semi-flat or concave morphology, raised in place of their contact and leaning against each other, “pressing” each other from opposite directions, occupying the dominant part of the form, usually in the middle of it. The dome, on the other hand, has a dominant rounded (convex) shape without a sharp crest.

The geomorphometric parameters for the characteristics of the studied landforms were adopted from descriptions of the analogous domed forms of relief: hydration forms [18,48], gypsum tumuli [36,37,67], drumlins [82,83,92], and granite A-tents [64,66]. Some parameters were modified and the new ones were also introduced as described below. The geomorphometric description of the landforms was carried out during both field and office work and was adapted to their convex morphology.

During the office work, photogrammetric data and data obtained as a result of their further processing, such as 3D and 2.5D models [93], orthophotomaps, point clouds with extension *.las* and DSMs were collected and elaborated. These works mainly involved ArcGIS, Photoscan, Excel and Corel Draw X9 programs.

Work in the ArcGIS program (Esri, Redlands, CA, USA) began with the transfer of the extent line for each of the 74 identified hydration forms to the orthophotomap of the area (3 forms were excluded from the analysis because of the lack of photogrammetric data; see Table S1). Based on the extent of the form, lines of the longest axis (length of the form, *a*—longer axis; Figure 3) were drawn and measured on the map similarly to Spagnolo et al. [82] and Maclachlan and Eyles [83], as the longest straight line possible within the mapped forms area. Then, the width of the form (*b*—short axis; Figure 3) perpendicular to the *a* axis was drawn and measured [82,83]. The crest lines through the points of maximum curvature of the majority of contours were also marked (Figure 3) [92].

An orientation of the axis *a*, i.e., elongation of the form, was computed to acquire the azimuth of elongation orientation *Az* of every form and, on the basis of these measurements, to generate a rose diagram. On the basis of the DSM, the Zonal Statistic as Table tool [94] (pp. 327, 349) was used to measure the values of elevations (in m a.s.l.) marked by h_{\max} and h_{\min} (Figure 3). Value h_{\max} is the peak at the highest elevation point (usually located in the middle of the form) while h_{\min} is the lowest elevation point of the hydration form within its extent. The relative height of form h_r is understood as the form altitude range and is the result of subtraction h_{\min} from h_{\max} (see [84]). This value does not take into account the hillslope of the terrain surface, which at Dingwall is generally minimal. When the forms were overgrown with vegetation, the covered part was excluded from the calculation of relative height.

As part of the statistical analysis realized in the Excel program for all the calculated parameters (Table 2), a simple linear regression analysis was performed to reveal the possible regular relationships between these parameters [95]. The regression lines were generated and the Pearson correlation coefficient was calculated. For the values: *a*, *b*, h_r , the regression line was fixed at a point (0,0) in the coordinate system to obtain a more realistic equation of their mutual dependence. All the values (*a*, h_r , *B*, *C*; see below) were used to create their frequency distribution diagrams (histograms). They were further analyzed in order to select or distinguish the characteristic groups that best reflect the real state.

The length and width of the hydration forms were used to calculate the coefficient of circularity (*C*), characterizing the degree of elongation according to the formula [18,36]:

$$C = (a - b)/a \quad (1)$$

It was calculated in a similar way as the so-called flattening in case of elliptical objects [67]. For its value closest to 0, the form is the most round; for the value closest to 1, the form is the most elongated. The coefficient of circularity is a parameter analogous to the elongation (degree of elongation, E), calculated as the ratio a/b often used in the description of similar forms of relief [81,84]. The relationship between both parameters is described by the formula:

$$C = 1 - 1/E \quad (2)$$

The ratio called bulge degree (B) was calculated as in the case of drumlins [84] by the formula:

$$B = b/h_r \quad (3)$$

It was used in order to determine the convexity of hydration forms quantitatively. The increasing value of the ratio b/h_r informs about a higher flattening.

A detached rock layer in the studied forms is characterized by a thickness (e in Figure 3) measured perpendicularly to the surfaces of this layer, as in the case of the A-tent landforms [64] or gypsum tumuli [18,36,67]. Based on the field measurements and detailed cross-sections, its thickness was determined, and when *.las* data were not available, only field measurements were taken into account. Cross-sections were made thanks to the *.las* format data generated in Photoscan (Agisoft LLC, St. Petersburg, Russia) and analyzed in the ArcGIS program (Esri, Redlands, CA, USA). The cross-sections were drawn, as shown in Figure 3, in the ArcGIS program using the Stack Profile tool. Where the rock layer thickens considerably toward the margin of the form, the thickness measured in these places was not considered.

Additionally, the orientation of entrances to an internal space or cave of hydration forms was analyzed. The entrance is defined as breaking the continuity of the detached rock layer, revealing the interior of the form. Some of the internal spaces of the forms are large enough for direct adult human exploration and therefore represent hydration caves [27,96], or, strictly speaking, proper caves sensu Curl [96,97]. On the orthophotomap, the upper edge of the entrances was commonly seen as a more or less long and straight line (entrance line; Figure 3). These lines were marked and their orientations were determined to detect some regularities of their orientations and a possible influence of the structure of bedrock on entrance formation. Only the entrance lines that show the minimal length of 0.30 m or more were marked. In cases where the lines were curved, they were approximated to the straight lines, while in the case of an entrance creating two distinct lines, the azimuths of both lines were measured separately (see Figure 3). The influence of the bedrock structure on the development of entrances was examined by tracing the fractures and layering visible in the quarry and comparing their orientation with the orientation of the entrance lines. Entrance lines were used to mark the azimuth of the entrance to the cave or cavity as generally normal to these lines. The azimuths directed out of the internal space of the forms were calculated and analyzed statistically.

3.2.2. Analysis of Structural Elements

The characteristics of the structural elements included the mentioned layering and fractures. They were documented in order to recognize their relationship with the morphology of the hydration forms (their elongation, orientation of entrances).

The strike and dip of the gypsum-anhydrite layers were measured directly in the quarry, and the strike of the layers visible in the bedrock was traced and documented as lineaments on the orthophotomaps in the ArcGIS program (Esri, Redlands, CA, USA).

Similarly, the fractures were both measured directly and traced using the orthophotomap in the ArcGIS program (Esri, Redlands, CA, USA). Attention was paid to fractures showing the features of systematic joints and master joints [98]. Traces of such fractures or joints were recognized on the orthophotomap and marked on areas of the quarry where they were best seen. The tilt value of these structures was assumed to be vertical or nearly vertical, based on the direct field measurements and observations. Joints and fractures

measured in the quarry were analyzed on Angelier diagrams, whereas joint traces on the quarry bottom were characterized on rose diagrams [99]. The rose diagrams (in the ArcGIS program using polar plots), unlike the traditional ones, took into account the length of the fractures, which translated into a more realistic analysis. The description of the fractures was based on the terms and classifications presented by Peacock et al. [100].

To characterize the deformation a rock has undergone to give convex hydration forms, we attempted to determine the direction of the maximum lateral (horizontal) expansion (or extension) within this surface layer (Figure 3) in a similar way as Ericson and Olvmo (Figure 9 in [66]) designated the direction of extension in A-tens (see also [65]). The maximum lateral expansion (MLE) was marked as normal to the line of the crest of the form. The wavy-shaped crests were approximated to straight lines and MLE was assumed to be normal to this line. In many cases where precise determination of the direction of the MLE was difficult or impossible, it was marked arbitrary. The relations of MLE to elongation of the forms were investigated by determining the angles between both directions.

Attention was paid to the fractures occurring on the surface and in the vicinity of the hydration forms. Their orientations were measured to reveal the influence of master joints on the development of fractures within hydration forms and in relation to the direction of MLE [85]. The intersections of fractures were studied to determine the order of their generation [100,101]. In addition, the surface density of fracture traces [102] in 3D space, F_D , was calculated for every form according to the modified formula [85] and similar to the trace density formula [86]:

$$F_D = \frac{\sum Ls}{P} \quad (4)$$

where:

$\sum Ls$ —sum of the length of the fracture traces within the hydration form surface measured in 3D (m)

P —surface area of hydration form (m^2)

4. Results

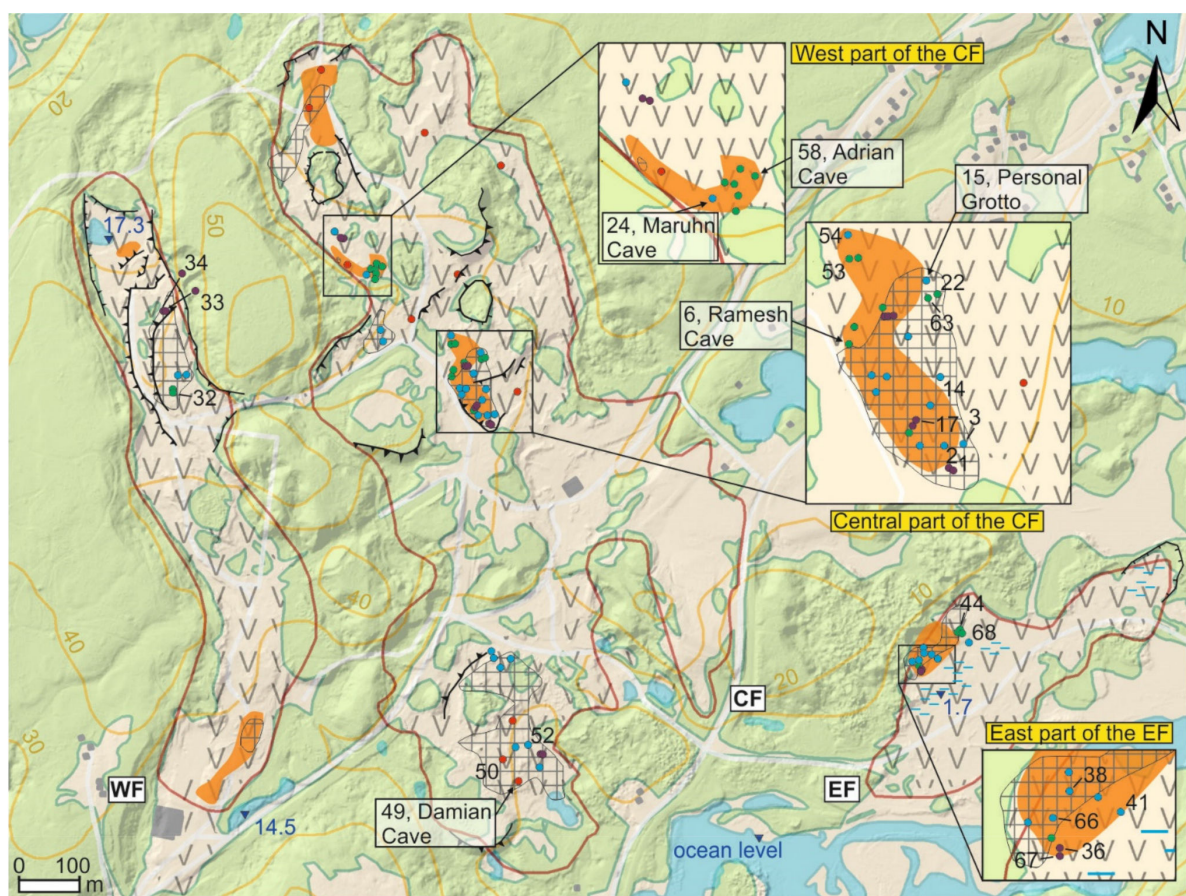
The generated photogrammetric models and their survey, taking into account field observations and statistical analysis of the collected data, provided the basis for morphological and structural analyses of the hydration forms. Photogrammetric data include several good-quality 3D and 2.5D models of hydration landforms (see Figure S1 for more details). A map of the quarry with marked traces of fractures and layers, as well as the extent of hydration forms, is a main result of the work (Figure S8). The complete documentary and statistical data are presented in Supplementary Materials (Table S1, Figures S1–S9), as well as on video materials available on Youtube.com (profile name: hydration caves), which present a comprehensive view of the hydration landscape. The photographic and cartographic documentation of the studied hydration forms is presented both in Supplementary Materials and on the website [103].

4.1. Morphology of the Quarry Bottom

The quarry, divided into three parts: WF, CF and EF (Figures 1 and 4), occupies about 78 ha at an altitude of 0–53 m a.s.l. with the lowest terrain in the EF and south of the CF. The rocks are very well exposed and only in places covered with low sparse vegetation. Young trees up to 1.5 m high grow in the oldest parts of the exploitation fields, containing more weathering debris. Small ponds occur in several places and the EF is partially covered by periodic wetlands (Figures 4 and S3).

At the end of mining operations in 1955, the bottom of the quarry, mostly cut in the anhydrite bedrocks, was left generally flatted and remained exposed to weathering. Hydration domes and ridges (“pressure blisters” and “pressure-ridges”) growing at the quarry bottom, as well as already destroyed ones, were observed as early as 1969, testifying to their earlier development [104]. A present-day rough, uneven relief of the rocky bottom is mainly a product of expansive hydration of anhydrite due to the reaction with waters

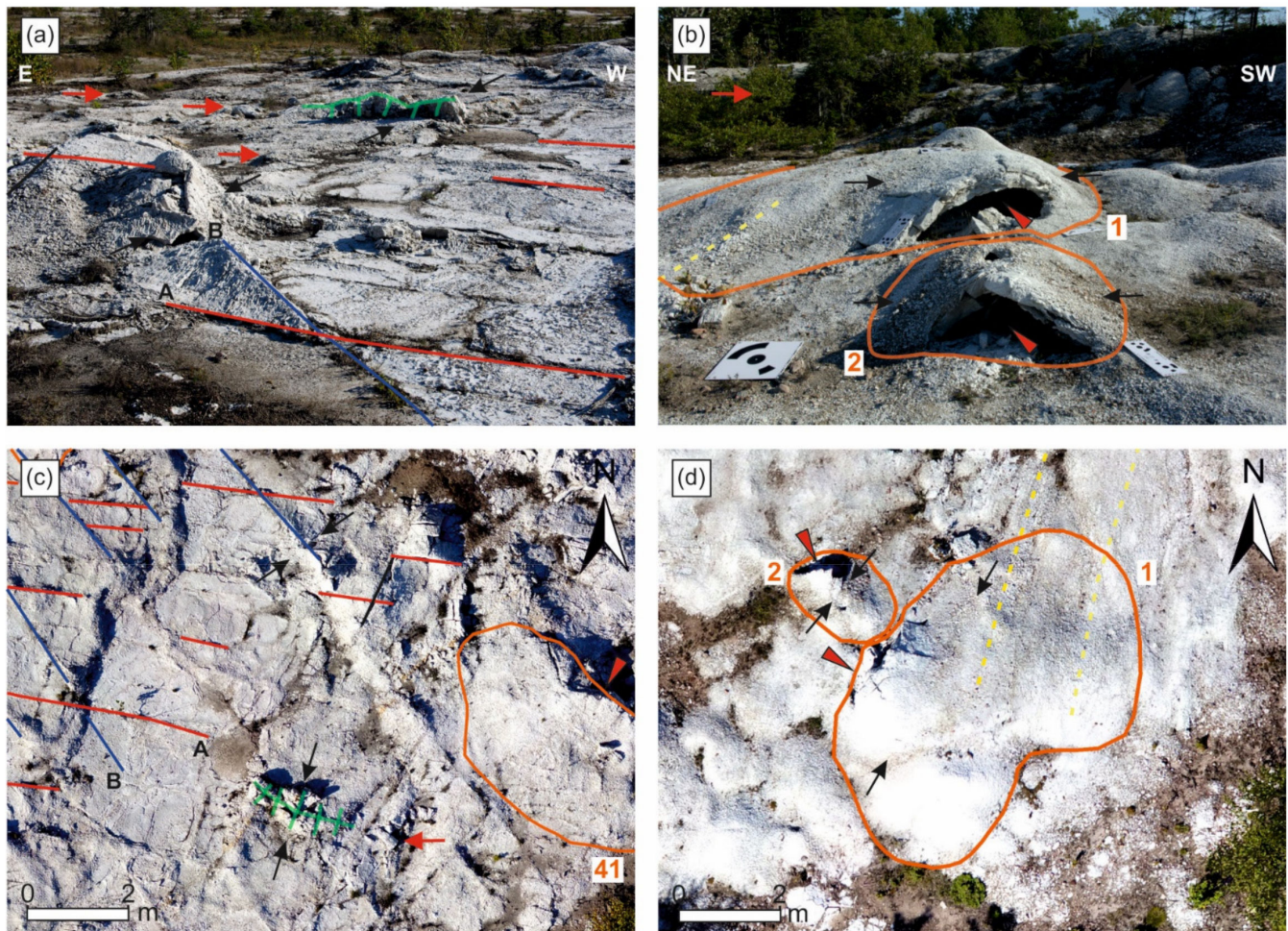
of meteoric derivation. This process has been acting since 1955 and from the 1930s at the earliest—in places where the first gypsum mining was started. The relief produced by present-day dissolution (karren, [78]) is of minor importance. The created hydration landscape dominates in many parts of the quarry (Figures 2, 4 and 5a,b). The large hydration domes and tepee-shaped forms, with a relative height of above 0.5–1.0 m and an extension in a plan view up to several and a dozen meters, are the most distinctive products of expansive hydration. Seventy-seven of these forms were documented, of which three were only partly measured and did not have photogrammetric records (Figure 4, Table S1). Within the examined forms and in their vicinities, numerous fractures are present, including fractures belonging to the master joint system. The formation of new fractures, evidently younger than the master joints, was documented by photographs (e.g., Figure 4 in [8]; Figure 5 in [9]). They have apparently been formed due to present-day weathering, including anhydrite hydration [14].



Legend

- | | | |
|---|---|---|
| 22 hydration form identification number | extent of the quarry | periodic wetlands |
| • very sparsely distributed hydration forms (at a distance of >25 m) | extent of joint traces documentation | roads |
| • sparsely distributed hydration forms (at a distance 5-25 m) | extent of layers traces documentation | ▼ 17.3 water level measured by GPS devise with RTK corrections in September 2018 [m a.s.l.] |
| • densely distributed hydration forms (at a distance 0.5-5.0 m) | ∇∇ gypsum-anhydrite rocks | areas covered with: |
| • very densely distributed hydration forms (at a distance of <0.5 m) | contours lines, interval 10 m | vegetation |
| | ↗ steep slope | waters |
| | ↖ rock cliff | buildings |
| | | other areas |

Figure 4. The map of 77 studied anhydrite hydration landforms at Dingwall (source of base maps: ArcGIS program (Esri, Redlands, CA, USA) and nsgi.novascotia.ca); forms mentioned in the text are numbered (full numeration is shown on the maps in Figure S3).



Legend

- 1 extent of the hydration form and its identification number
- ▶ entrance to the cavity
- - - traces of layers
- ↖ ↗ maximum lateral expansion
- — joint sets A (red) and B (dark blue) and other fractures (black)
- + + + pressure ridge
- small hydration forms

Figure 5. Hydration relief of the Dingwall site; (a,c) part of the quarry bottom with visible bulges, fractures and a pressure ridge; note unnumbered forms not measured in this study. (b,d) Dome-like hydration forms with entrances to the inner cave (no. 1) and smaller cavity (no. 2); see Figure 4 for the location of the forms.

The rock surface of hydration forms is solid but also covered with loose gypsum-anhydrite weathering debris composed of cm-mm-sized sharp-edged rock fragments [8]. This debris develops relatively rapidly with time, which is very well seen in the photographs taken several years apart (Figure 2d,e). In the oldest parts of the quarry, initial soil and vegetation have developed on the debris, forming a several cm thick weathering mantle. In some parts of the quarry, this weathering mantle (regolith) has been cut by a network of erosional furrows (Figure S8). Because of the presence of the weathering mantle, debris and vegetation, the structure of the bedrock is entirely invisible in vast areas of the quarry.

4.2. Distribution of Hydration Landforms

The hydration landforms were recorded only in a few parts of the quarry and were presented on a topographic map (Figure 4) and a satellite map (Figure S3). The distances between the forms ranged from less than 0.5 to more than 25 m. Considering the following three limits of distances—0.5 m, 5 m, and 25 m—four groups were distinguished according

to the range of a distance between the forms: very sparsely (14%), sparsely (40%), densely (26%) and very densely (19%) distributed forms (Figure 4). A group is a set of at least two forms. Two close to each other forms from the CF (no. 1 and 2, Figures 4 and S2) are an example of a very densely distributed hydration form (Figure 5b,d). The highest number of forms (31) occurs in the middle of the CF, but they vary, from very sparsely to very densely distributed (Figure 4).

4.3. Shape and Morphometry of Hydration Landforms

The hydration forms show a diversified shape in a plan view. Most of them are quite regular and more or less rounded, but some of them are irregular in shape (Table 2). Taking into account the coefficient of circularity (Table S1, Figure S5), the more regular forms are divided into round, slightly oval, oval, slightly elongated, elongated and strongly elongated (Figure 6). The oval and slightly elongated forms constitute 42% of all examined objects, and 8% of the forms are irregular in shape (7 forms, e.g., Figure 7i). The latter group is the least numerous (Figure 7b) and has an uncommon geometry without any clear elongation orientation (Figure 7i, Table S1).

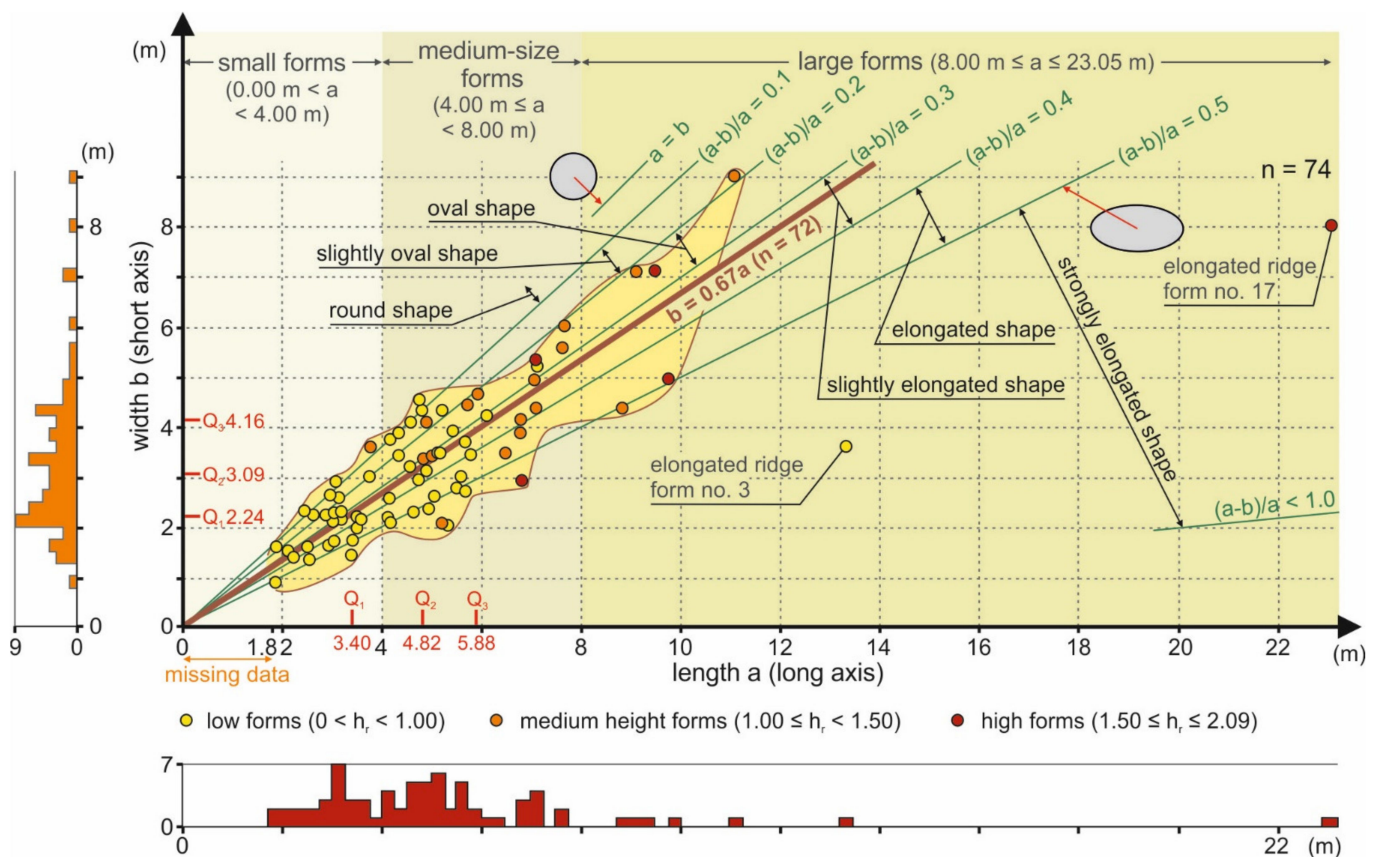


Figure 6. Diagram showing relation of width to length in 74 anhydrite hydration landforms divided according to h_r value and a value, showing the diagram areas for different values of the coefficient of circularity $(a - b)/a$, first (Q_1), second (Q_2) and third (Q_3) quartile of a and b value, as well as showing regression line of the width and length relation for 72 hydration forms (yellow area), excluding two elongated ridges, supplemented by frequency distribution diagrams of the width and length. Further explanations in the text.

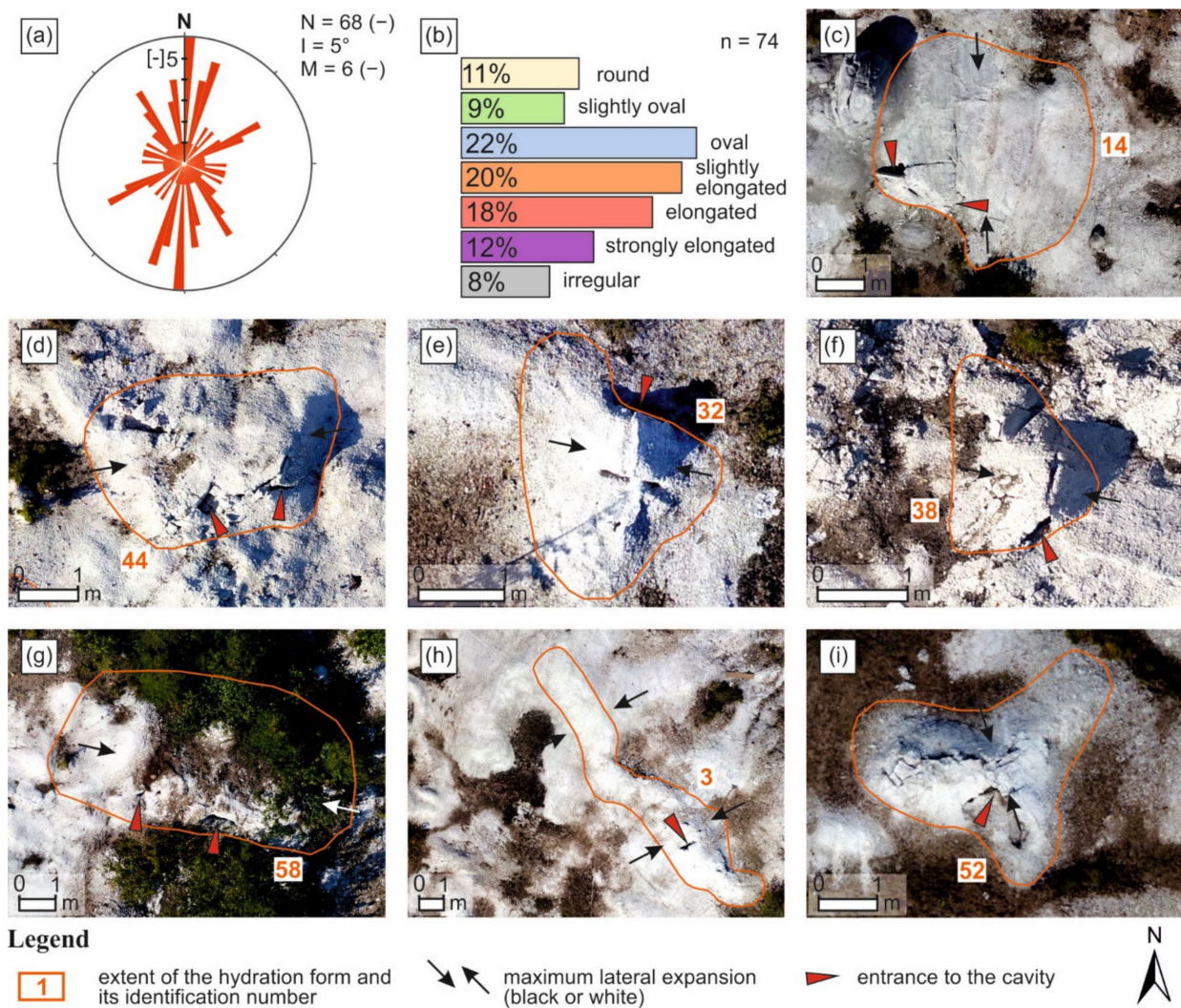


Figure 7. Characteristic of the elongation of the hydration forms at Dingwall; (a) rose diagram of azimuths of form elongation (Figure 3; N—total number of the forms, I—azimuth interval, M—number of forms represented by a circle radius); (b) frequency distribution of forms divided into groups according to coefficient of circularity (Table 2), including irregular forms (Figure 6); (c–i) examples of variously elongated forms and irregular form presented on orthophotomaps: (c) round form; (d) slightly oval form; (e) oval form; (f) slightly elongated form; (g) elongated form; (h) strongly elongated form; (i) irregular form.

The most dominant azimuths of the landform elongation have values of 0–5°, 15–20°, 65–75°, and 140–150° (Figure 7a). These dominant orientations poorly coincide with the orientations of master joints, although these joints create as many as five distinct sets (see Section 4.6.1). Additionally, direct field observations indicate that, despite the presence of the characteristic-oriented master joints in the particular parts of the quarry, the forms occurring there show rather random elongation (Figure S8).

Elongation of the landforms shows oriented relations with direction of MLE and is perpendicular to it, with an accuracy of ±5°, in 46% of forms, and parallel to it, with the same accuracy, in 29% of forms.

The relationship between landform elongation and the strike of layers is unclear. There is a certain convergence of dominant orientations of elongation and layering in several hydration forms, e.g., in the southern part of CF. In places, the traces of strike are perpendicular or at some acute angle to the elongation of the forms (Figure S8).

The measured lengths of the landforms range from 1.86 to 23.05 m (Table 2, Figure 6). The measurements clearly showed that the longer the forms, the less frequently they occur (Figure 6). From the length frequency distribution, the limits of 4 and 8 m were established, situated in intervals of occurrence of low frequency length values, as the most closed to natural limits for dividing the forms according to sizes into the following groups: the small, the medium-size, and the large forms (constituting 34%, 57% and 9% of all the objects, respectively; Figures 6 and S5). Among the 74 measured hydration forms, the largest (longest) form is 23.05 m in length and up to 8.02 m wide (no. 17, Tables 2 and S1, Figures 4 and S2). It stands out from the others with its strongly elongated shape, the morphology of a pressure ridge, a tepee-like shape in cross section, and an outstanding relative height of 2.08 m. On the other hand, the shortest documented form is 1.86 m long and has almost the lowest relative height of 0.35 m. It is a form with a distinct tepee shape and characteristic concave bending of detached layers (no. 66, Tables 2 and S1, Figures 4 and S2).

According to general shape, 52 dome- and 25 tepee-like forms were distinguished, representing 67.5% and 32.5% of all the studied objects (Table S1).

The relative heights of the landforms range from 0.33 to 2.09 m (Table 2), and half of the recorded values range from 0.56 to 1.05 m. Again, using the frequency distribution of the relative heights, two limits of 1.0 and 1.5 m were determined within the low-frequency intervals on the histogram, and considering these limits, the forms were classified into three groups: the low forms (72%), the medium height forms (22%), and the high forms (7%) (Figures 6 and S5). The highest hydration form shows a relative height of 2.09 m and is characterized by a domed shape (no. 49, Figures 4 and S2, Table S1). Such a large height of that form corresponds to the largest area of the internal cave, 29.4 m² (the Damian Cave [61]).

The width of the landforms appears to change proportionally to their length, except for the most elongated forms represented by the two pressure ridges (no. 3 and no. 17, Figure 6). Similarly, the relative height seems to change proportionally to both the length and width of the forms (Figure S6). The linear correlation between the discussed parameters can be expressed by the following equations, characterized by relatively large values of correlation (Pearson) coefficients (r), indicating moderate correlation (Figures 6 and 8) [95] (p. 529).

$$b = 0.67a \tag{5}$$

$$h_r = 0.16a \tag{6}$$

$$h_r = 0.23b \tag{7}$$

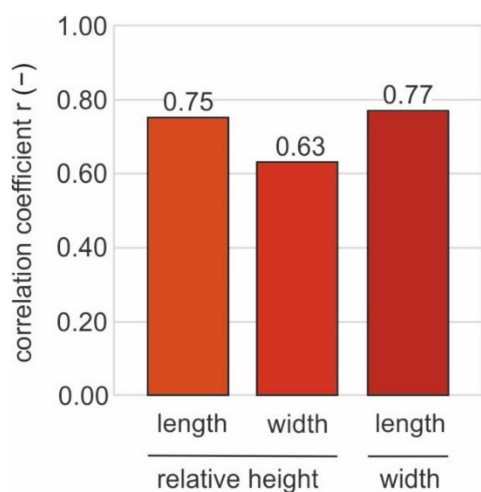


Figure 8. Correlation coefficient r for relations of relative height with length and width and also for the relationship between length and width computed for 74 anhydrite hydration forms.

Stenson [48] obtained the best correlation between the height and the width of the forms (expressed by the ratio height/width ≈ 0.16 , $n = 69$). Our data suggest the best correlation between the length and the width (Figures 6 and 8).

The frequency distribution of b/h_r ratio shows that the average bulge degree of the studied forms is 4.28 (Table 2, see Figure S5). This parameter has an exceptionally high value of 8.58, indicating the least convex form, with a relative height ca. eight times less than its width (no. 68, Figure 9a, Table S1). In spite of its flatness, this form has an internal hydration cave, which is a proper cave with a proper entrance sensu Curl [96,97,105], i.e., an open cavity large enough to crawl inside by a man. On the other hand, the lowest value of bulge degree 1.82, indicating the greatest convexity, is recorded in the typical tepee-shaped form with a relative height of only ca. two times less than its width and created by two rock slabs leaning against each other (no. 15, Figure 9b and Figure S2, Table S1). This strongly bulged form also currently has an internal cave (in 2019), reaching 1.27 m in height (the Personal Grotto, Figure 9b). The height of this cave continues to rise (Figure 13 in [9]).

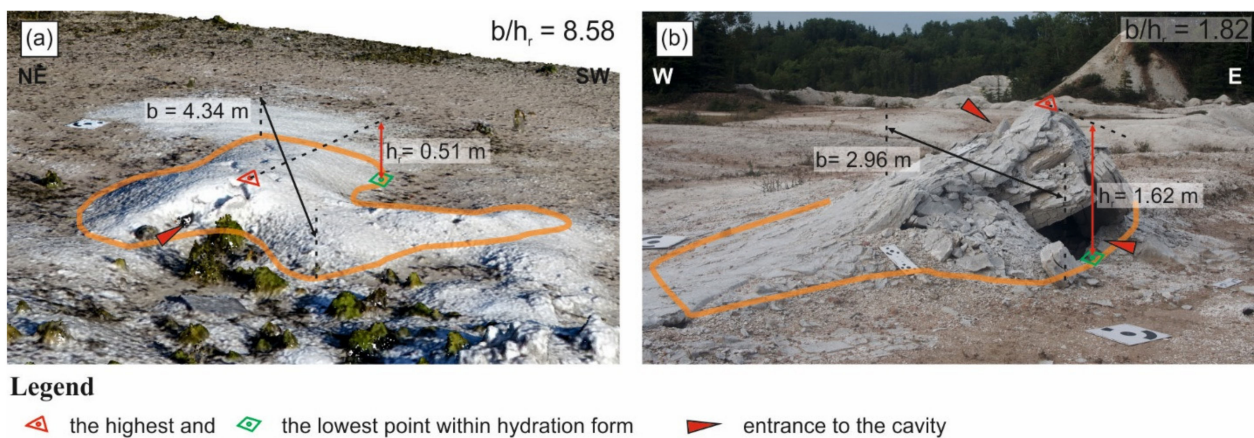


Figure 9. Anhydrite hydration landforms with extreme values of bulge degree (b/h_r ratio); (a) form no. 68 with the highest value of bulge degree visible on the 3D model; (b) form no. 15 with the lowest value of bulge degree. See Figure 4 or Figure S3 for the locations of these forms.

Generally, it can be noticed that, on average, the tepee-shaped forms have a slightly higher convexity (average b/h_r is 3.69) than dome-shaped forms (average b/h_r is 4.51; see Figure S5). The degree of bulge does not correlate with the length of the forms in a linear manner (Figure 10a). Such a correlation is also weak between bulge degree and width (Figure 10b) and bulge degree and coefficient of circularity (Figure 10c). Generally, it is seen that the higher convexity is reached by forms with a smaller length (Figure 10a), and the lower bulge degree by forms with a smaller width (Figure 10b).

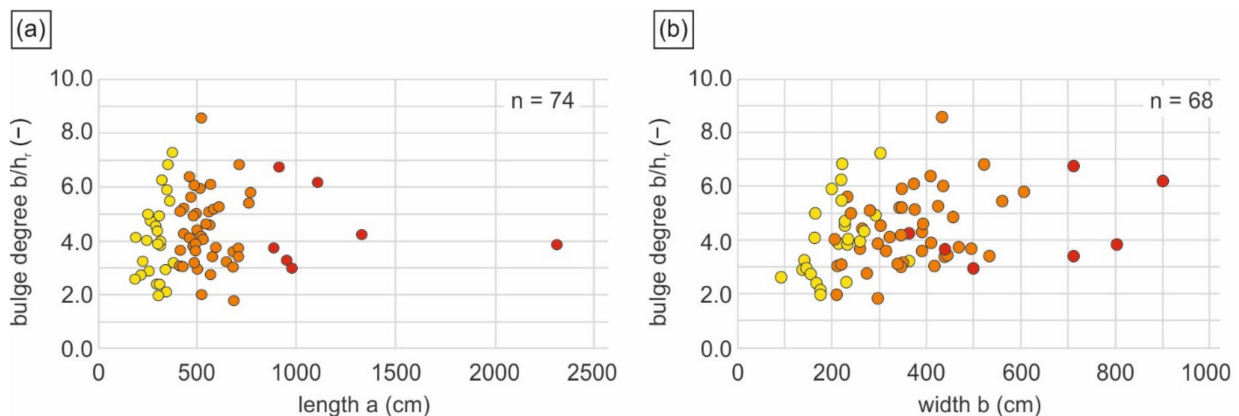


Figure 10. Cont.

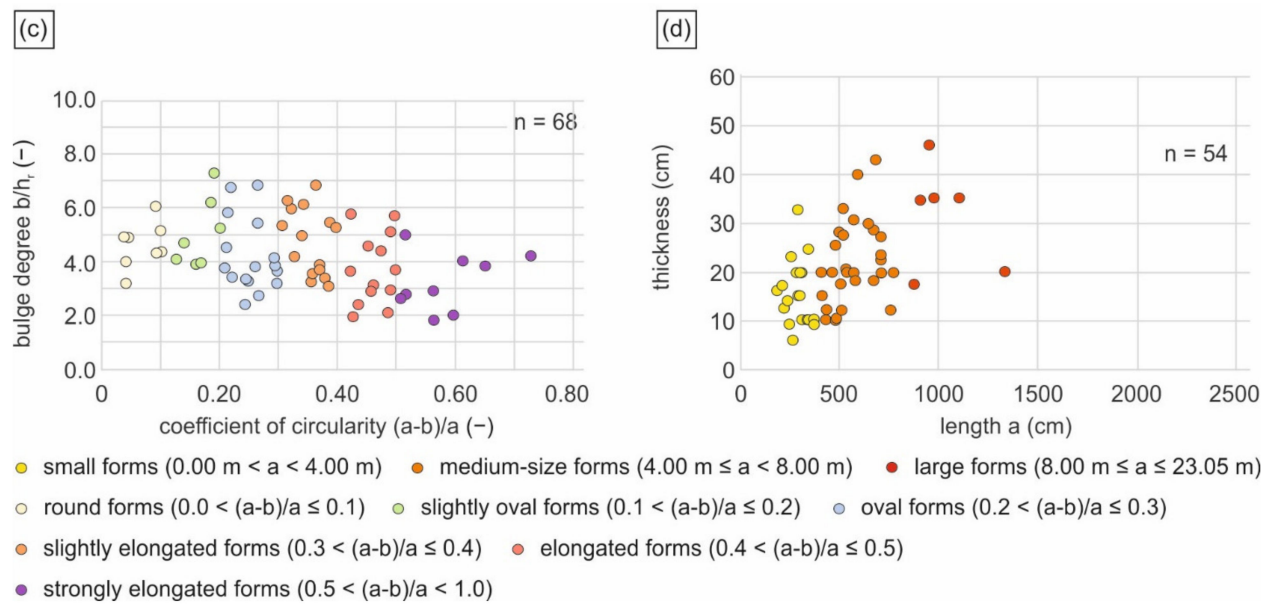


Figure 10. (a–c) Dependence of bulge degree on length (a), width (b) and coefficient of circularity (c) of the anhydrite hydration landforms (Figure 3); (d) dependence of thickness of detached layer on length of the hydration forms. Diagrams (a,b,d) take into account the size groups of the forms according to length of the long axis a and diagram (c) takes into account the groups of the forms according to coefficient of circularity.

4.4. Detached Layer

The averaged thickness of the detached and uplifted gypsum-anhydrite layer for 54 hydration landforms ranges from 6 to 46 cm, with an average value of 21 cm (Tables 2 and S1, Figure S4). It is generally observed that the greater the length of the forms, the greater the thickness of detached layers (Figure 10d). There is no visible difference between the thickness of the detached layer in the tepee- and dome-shaped forms.

4.5. Inner Cavity

Documented internal cavities of the studied 74 hydration landforms involve 48 proper caves, including 43 caves with a proper entrance [96,97]. The other cavities are too small to be a proper cave or cannot be verified whether they are such caves because of restricted access to their interior. The lengths of the documented 47 caves and cavities are from 0.70 to 8.87 m, and the range of the heights is from 0.28 to 1.35 m (data from 2019, in 2008 the length of the Ramesh Cave was larger—its floor space was ca. 10.7×6.6 m and it was 1.10 m high, which makes this cave the largest known hydration cave in the world) [8,61]. The largest cavities were identified in domed forms; the tepee-shaped forms had a relatively smaller inner space. The ceiling is generally flat, with a slightly rugged surface, but it also shows fractures and thin protruding rolled rock layers. Larger rock fragments fell from the ceiling, crystalline gravel derived from the till and leaves cover the bottom. Caves are predominantly opened only from one side; rarely, they have two entrances (Figure S2). Inlets leading to several caves are too narrow for an adult man to crawl inside.

The entrance lines (with the minimal length ≥ 0.30 m) were determined in 69 of the 74 hydration landforms (Figure 11). The length of the entrance line marked on the map (in six cases—two distinct lines) ranges from 0.30 to 4.52 m (Table 2). A single entrance documented by the entrance line occurs in 48 forms, two entrances appear in 20 forms and three entrances in one form. They lead both to proper caves, enabling humans to enter, and to smaller cavities.

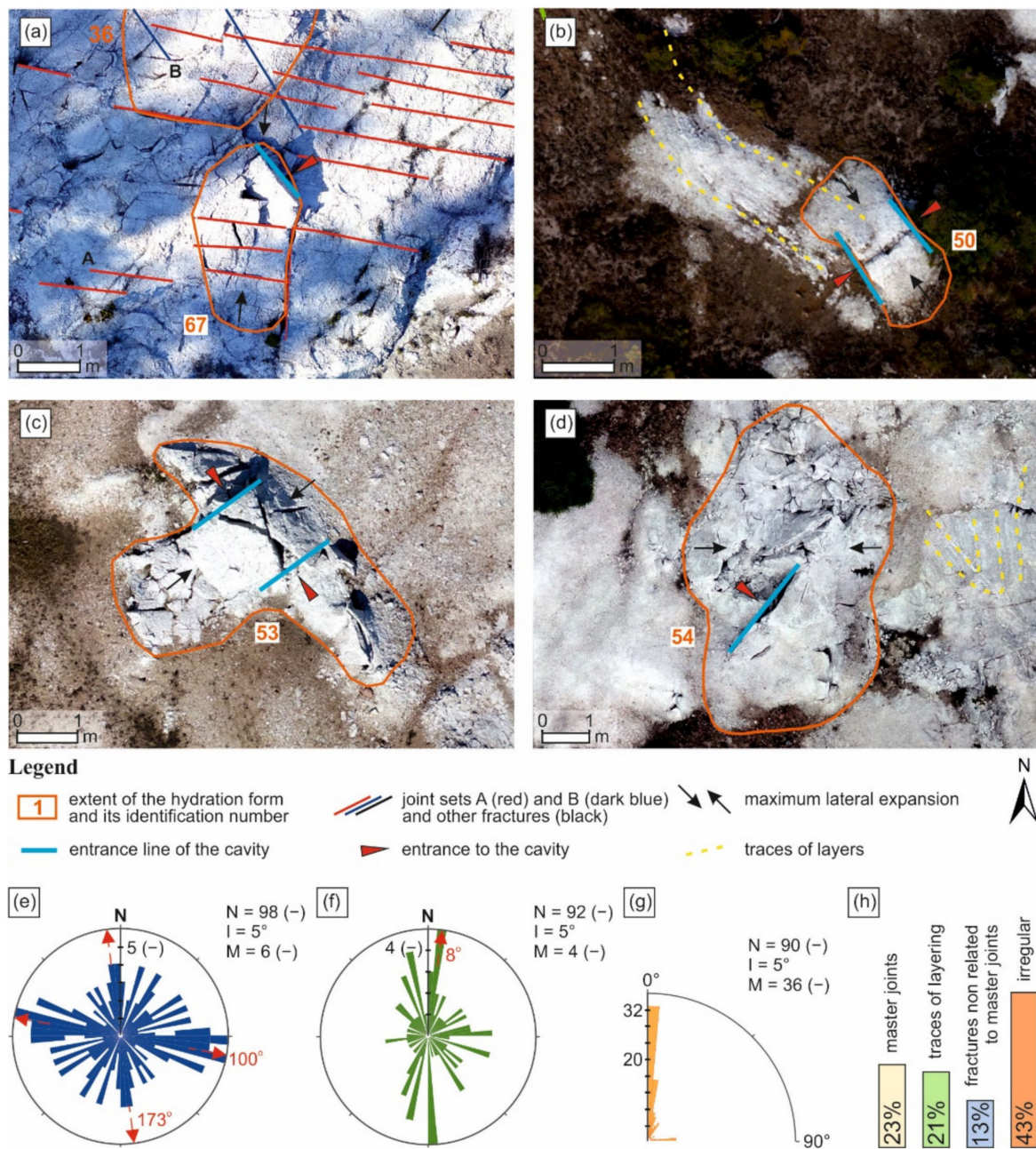


Figure 11. Morphometric features of entrances to hydration caves and cavities and their relation to master joints and layering; (a–d) exemplary anhydrite hydration landforms showing parallelism of the entrance lines (Figure 3) with master joint system (a), layering (b), and fractures within form related neither to master joints nor layering (c) and the form with lack of any regular relations between entrances and above features (d); (e,f) rose diagrams of the orientation of the entrance lines (e) and directions of the entrance (from inside the form to the outside) (f) with red arrow symbolizing dominating azimuths (N—total number of the forms, I—azimuth interval, M—number of forms represented by a circle radius); (g) rose diagram of the values of angles between entrance lines and directions of MLE (Figure 3); (h)—frequency distribution of entrances according to coincidence (more or less common orientation) of entrance lines with listed linear features and to lack of any visible relations with these features (irregular). The master joints and layering in the vicinity of forms illustrated in (c,d) are seen in Figure S8.

In 23% of cases, the entrance line coincides with some master joints in the vicinity of the form and in 21% with layering (Figure 11h). However, entrance lines are also more

or less parallel to the other fractures, probably generated mostly by expansive hydration (Figure 11h). The rose diagram of entrance lines azimuths points out two dominant orientations: more common 100° and less common 173° (Figure 11e). The former orientation appears to coincide with the master joints set A (Figure 12a–c,e,f) and the latter with the common strike orientation (Figure 11d,f). Many entrance lines are irregularly oriented (Figure 11d,h). Azimuths of the directions of entrances are variously spread out, but the north direction is the most numerous (Figure 11f).

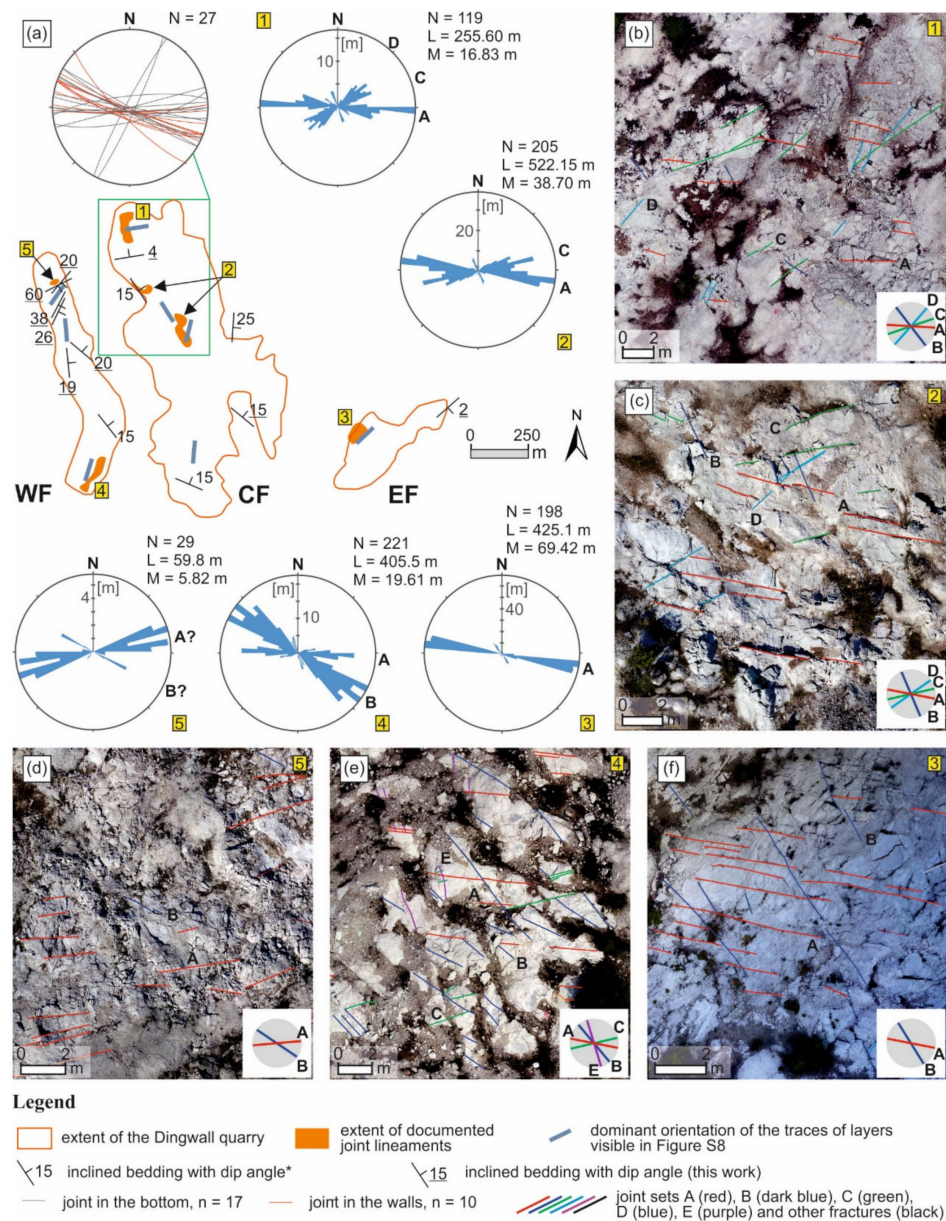


Figure 12. System of master joints recorded in the quarry at Dingwall; (a) joints measured in bottom and walls of the quarry within area marked by green rectangle (shown on Angelier diagram, upper hemisphere; upper left, N—number of measurements) and joints traces documented in particular parts of the quarry (shown on rose diagrams numbered 1–5; N—total number of fractures, L—total length of fractures, M—maximum length of a circle radius) together with dominant direction of layering; (b–f) fragments of the orthophotomap showing characteristic sets of joints A–E documented in particular parts of the quarry marked on figure (a); each set is marked with the same characteristic color on the map and in circles at bottom right. Note the rotation of main joint set A across the quarry. In all the figures (a–f), north is in the same orientation as in figure (a); *—data after Neale [71].

Most commonly, the entrances have opened with entrance lines parallel to the MLE, which means that they are simultaneously perpendicular to the crests of the forms (Figure 7e). In some cases, the entrance line is oblique or rarely perpendicular to that direction (Figure 11g).

4.6. Fractures and Layers

4.6.1. System of Master Joints and Fractures

Within the entire quarry, more than 754 fractures and traces of fractures were documented as lineaments and most of them represent joints (Figure S8). Well-developed systematic joints with an approximate vertical orientation were identified in six areas (Figure 4). These joints appear at a distance from ca. 0.5–2.0 m up to 10.0 or more meters (Figures 5a,c, 11a and 12). Twenty-seven joints and fractures were measured directly in the quarry (Figure 12). Azimuths of joint traces show significant similarity in orientation, permitting recognition of three main sets A, B and C and two less pronounced sets D and E (Figure 12). From one to four of these sets were observed to occur together in one place (Figure 12b,c,e). Joint set A (red in Figure 12) is commonest and has changeable azimuths and an average acute angle in relation to set B (dark blue line). The fractures measured in the north of the CF (Figure 12a, upper left) are mainly equivalents of joint sets A and C recognized in this part of the quarry (areas 1 and 2; Figure 12a). The joint system tends to cut the layering at angles of 40–90°, except in the northernmost part of the quarry (Figure 12a).

4.6.2. Fractures of Hydration Forms

Fractures in the detached rock layer cut it at right and oblique angles or parallel to its top or base. They represent both extension and shear types occurring with the opening between fracture walls and without any space-separating walls. The landform surface is dominated mainly by transverse fractures parallel to the MLE direction, as well as longitudinal, equally frequent ones perpendicular to this direction (Figures 3b and 7c,e,f). Irregular fractures (oblique to the MLE direction, Figure 3b) occur in a smaller amount than the abovementioned ones, but they can still be found in 34 of the 74 investigated forms. Spherical (Figures 3b and 5a,c) and radial fractures (form no. 22, Figure S2) are by far the least common. Spherical fractures are associated with the effects of spheroidal weathering of anhydrite blocks subjected to hydration [14], described elsewhere as “cannonball” structures [106].

The presence of joints cutting the forms and continuing outside of them representing the above-described sets A–E are characteristic of 28 of the 74 examined forms. Such joints are excellently visible in the exemplary form in EF (Figures 11a and S8).

The surface density of fractures in the detached rock layer (recorded in 69 forms; five forms were without visible fractures) ranges from 0.04 to 3.38 m/m² (Table 2, Figures 13 and 14b). The areas of the quarry with the large impact of the master joints are characterized by a higher F_D value compared to other areas (Figure 13). For all the hydration landforms, regardless of whether they are connected with master joints or not, the density of fractures is only slightly larger for the tepee-shaped forms than for the dome-shaped ones (Figure 13). The highest average F_D is recorded in the SW part of the EF influenced by the master joint system, where one form is characterized by a plentiful amount of fractures and the largest recorded F_D of 3.38 m/m² (no. 67, Figures 4, 13 and S8; Table S1).

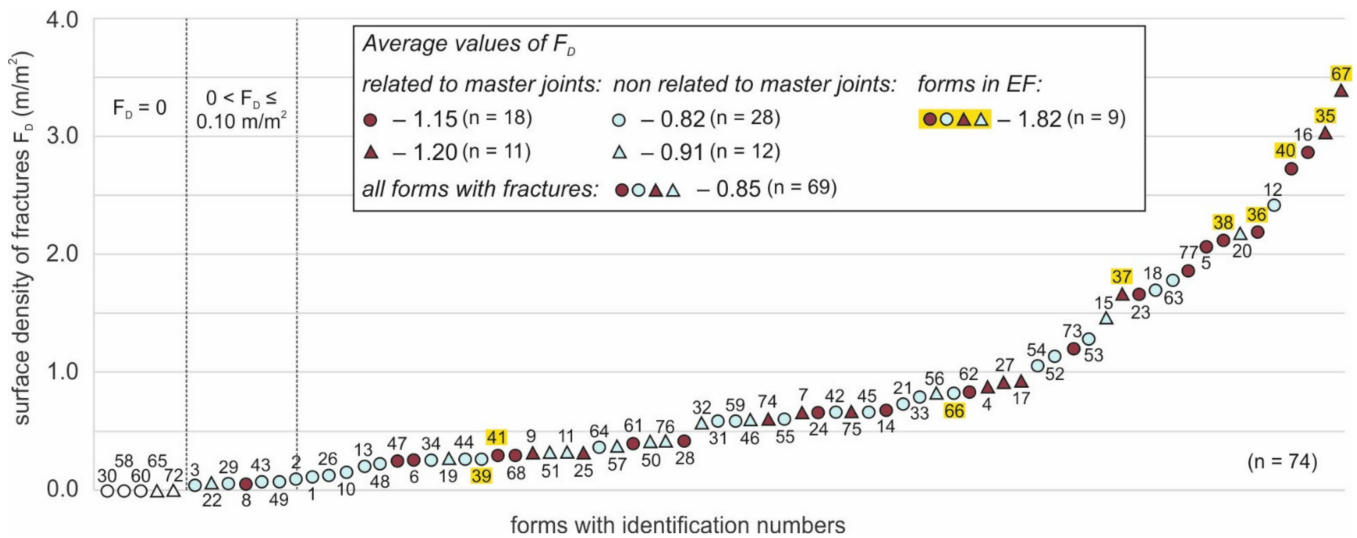


Figure 13. Fracture surface density F_D for 74 anhydrite hydration landforms taking into account dome-like shape (circle symbol) and tepee-like shape (triangle symbol), relation to master joints (claret color), lack of relation to master joints (blue color, further explanations in the text) and location in the EF of the quarry (yellow color). Average values of F_D are presented for both particular groups of forms and for all forms (n —number of measurements).

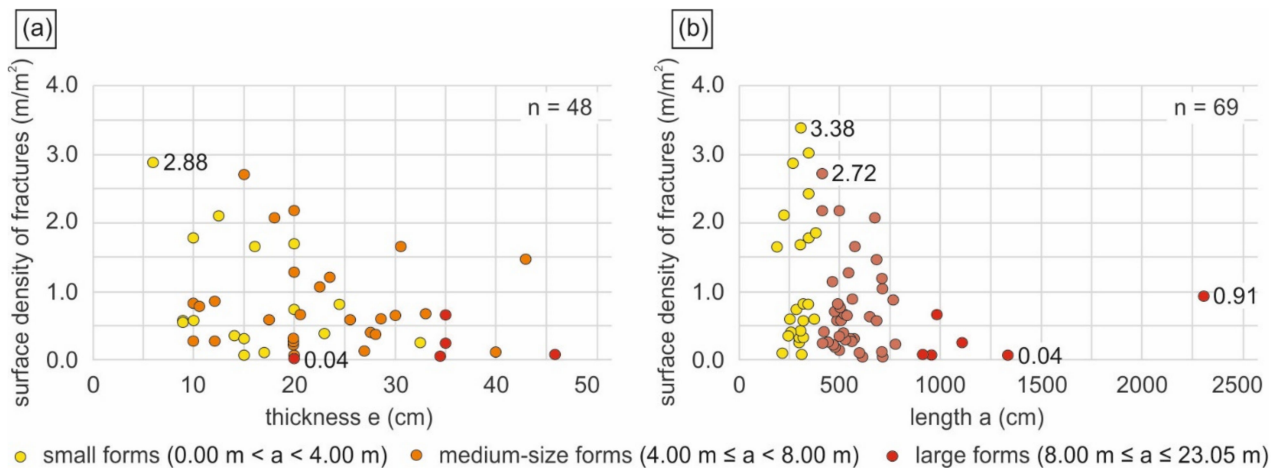


Figure 14. Dependence of surface density of fracture traces on thickness of detached rock layer (a) and on length of form (b), taking into account size classification of landforms according to length of axis a (Figures 3 and 6).

For 48 hydration landforms with measured thickness of detached layer, the density of fractures is variable, both very large and modest (Figure 14a). The lower F_D values are usually connected to greater thickness. For a thickness lower than or equal to 20 cm, the surface density can attain as much as almost 3 m/m², but if the thickness is higher than 20 cm, then this density does not overpass 1.66 m/m². Additionally, the relationship between F_D and the length of forms indicates that the smaller forms attain a higher fracture density (Figure 14b).

4.6.3. Strike and Dip of Layers

Traces of layering seen on the surface of the bedrock were documented as lineaments on the orthophotomap of the quarry bottom. Because the surface of the bottom is approximately horizontal, these traces represent strikes of the layers quite well. In some places of the bedrock, the layers are not visible because of the cover of weathering debris (e.g., in

surroundings of forms no. 24–28, 58 and 61 in NW part of the CF). Where seen, these traces are often oriented in one generalized azimuth but also run in a wavy manner, rapidly changing the orientation or even forming closed, oval structures (Figure 11d) [14,57]. The rose diagrams of the azimuths of the strike lines (lineaments) were created separately for eight parts of the quarry (Figure S8). The diagrams demonstrate that the dominant azimuths of strike are in the ranges of 16° – 48° and 147° – 172° . The dominant dip is to the east (Figure 12) [71].

4.7. Morphological Relationships and Structural Characteristics of Hydration Forms

4.7.1. Distribution

The expansive anhydrite hydration causes numerous and variable rock deformations at the bottom of the quarry. The accomplished observations demonstrate that the formation of the most distinctive convex hydration forms analyzed in this paper takes place rather in a non-uniform and irregular manner throughout the area, which is the opposite way of many ordered natural landforms, such as drumlins, patterned grounds, dunes or ripples showing regular spacing (e.g., [29,107]). In contrast to the ordered forms, the distribution of hydration forms is very variable; they occur with different densities throughout the quarry. Such a way of distribution, also noted in the other occurrences of dome- and tepee-like hydration landforms (Pisky, Walkenried), is not easy to explain. It seems that most of all, it is related to the features of anhydrite rocks controlling the anhydrite gypsification, which was discussed in a separate publication [14] but also to the topographic condition influencing the water migration paths.

4.7.2. Sizes

The values of the basic morphometric parameters for the 74 forms (length, width, relative height) show a relatively good (“moderate” [95]) mutual correlation for the relations: $h_r - a$, $h_r - b$, and $a - b$, characterized by simple Equations (5)–(7) (see also [48]). Such correlations suggest that the studied landforms, irrespective of their size, show fixed proportions of the mentioned parameters. Therefore, as in the case of the gypsum tumuli [36], their morphological evolution appears to follow the same or similar simple rules. In terms of shape, they are thus relatively regular landforms “printed” in the landscape, with nearly the same fixed proportions of the basic morphometric parameters (compare [84] p. 189).

The recorded variability of the measured basic dimensions can be explained by asynchronous initiation of the form growth, i.e., different ages of the forms [48]. Stenson [48] also supposed that the size of the forms depends on the depth of anhydrite hydration. Many of the studied objects represent so-called non-equilibrium landforms, i.e., landforms that are still growing or decaying [29]. Such forms usually show broader size ranges than more “stable” equilibrium forms, such as bedforms.

The dome- and tepee-like hydration landforms from Dingwall show specified variations in size and shape. They are limited in size, which is a characteristic feature of any landform defined as a discrete object [29,30]. We do not have quantitative data for the determination of their lower size limit, but it seems to be a few tens of centimeters or less (Figure 7 in [9]) [48]. Their maximum length attains ca. 23 m, a maximum width—ca. 9 m and a maximum relative height—slightly over 2 m. The large forms are, however, distinctly relatively rare, which is a typical feature of the majority of landforms [29]. Small- and medium-size forms with lengths in the range of 1.8 to 8.0 m are the most common and constitute 90% of the studied forms. A similar frequency distribution of lengths of hydration forms, with evidently rare larger forms, was documented at Pisky [57].

The basic dimensions of the hydration landforms at Pisky, Walkenried, Dingwall and the Alebastrovyye Islands sites are very similar. As evidenced by the ranges of their lengths, they reached a maximum value of more than 10 and even 20 m (Table 1). Heights are also on the same scale, reaching 2–3 m. In this regard, dome- and tepee-like hydration landforms are evidently globally scale-specific [29], although this conclusion is based on limited data from only fourth sites on Earth. A worldwide similarity of these hydration forms in sizes is

also present within the thickness range of the detached rock layer, which is from a few cm to nearly 50 cm at Dingwall and Walkenried [2,4], also in the Alebastrovyye Islands, as indicated by the drawings of forms [5], but at Pisky the thickness exceeds 50 cm in some cases reaching over 100 cm [18,58]. The slight differences in size parameters between the forms from the four discussed sites (Table 1) presumably reflect the environmental differences between the particular localities. Thus, the hydration forms at these sites are, to some extent, regionally or locally scale-specific [29].

4.7.3. Shape

During the development of hydration landforms, the rock layer rising on the bottom of the quarry creates a variety of shapes in a plan view, which were approximated to round, oval and elongated. The irregular shape formation in a plan view is manifested in a curved or even winding course of the erected rock and the formation of three arms, the crests of which do not give an unambiguous orientation to elongation.

Among the studied landforms, dome-like shapes, characterizing 2/3 of all the forms, predominate over the tepee-shapes. Stenson [48] distinguished blisters (domes), rounded-tents and A-tents (tepees) at Dingwall. We have found, however, that it is difficult to distinguish between the blisters and the rounded-tents and have classified both forms as dome-like forms according to the introduced criteria. Nevertheless, our almost 20 years of study of the site have revealed changes in the domed to tepee-like shape, as Stenson did [48]. However, we also noticed the constant domed shapes of many hydration forms during the same period of evolution.

The values of bulge degree (b/h_r) are variable. On the basis of the realized research, it appears that the tepee-shaped forms are characterized by the lower value of b/h_r , being more privileged to create steep surfaces and lift the top up. This, in turn, may indicate that the tepee-shaped forms could be created as a result of the action of larger expansive gypsification deforming the rock or deeper hydration, as supposed by Stenson [48].

Orientation of the crest line and direction of the MLE supply information on the way of creation of the particular hydration landforms and, among others, on the formation of their shape (reflected by the mentioned morphometric parameters). They provide information on the method of deformation or strain, which is mainly dependent on the place and course of anhydrite hydration and thus on the petrological structure of the bedrock [14]. In the later stages of the discussed landforms' development, the hydration and volume increase have apparently been concentrated in the vicinity of the erected forms within which, at that time, the hydration processes have slowed down [4] (Figure 15 in [9]) [28,49]. In the case of the studied landforms, particularly those with the tepee shape (Figure 3, right), the centers of accelerated volume expansion were located near the forms, somewhere on their opposite sides, indicated by the MLE direction. Such forms have risen by pushing the detached rock slabs against each other just from these opposite sides in a way similar to buckling [98]. The centripetal displacements of the rock slabs are well documented in the case of such tepee-like forms (Figure 43 in [4]) (Figure 6c–e in [9]) [49] proving this interpretation. Restoration of the course of the deformational processes is, however, not a subject of this paper devoted to the morphometric characteristics of hydration landforms.

4.7.4. Entrance to Internal Caves or Cavities

Entrances to the internal cavity of elevated hydration landforms are quite a common feature. They allow access to the interior of hydration forms and, in the case of 43 cavities being proper caves [96,105], entry and direct examination. The entrance within a detached rock layer was opened by the collapse or uplift of a part of the rock, commonly along with the flat fractures visible as a straight line in a plan view (Figures 2d and 11d). Many of these fractures existed before the uplift of the layer and represent some joint sets developed in the bedrock. This is clearly evident from the parallel orientation of many entrance lines and such joints (like set A) and also directly from the continuity of the fracture forming the entrance line with the joint in the bedrock near the form. These older fractures have easily

been widened or opened during the growth of the form, particularly due to the differential movements of the disconnected fracture walls and blocks on opposite sides of the fractures.

Moreover, the same orientation of the entrance lines and layering suggest that the fractures responsible for the creation of the entrances easily opened along with the bedding of the bedrock. Indeed, some newest fractures opening recently in the weathering anhydrite rocks are parallel to the layering (Figure 5b–d in [9]) and minor fractures parallel to the bedding are also noted (Figure 5i,l in [14]). However, it is remarkable that one-third of the entrances have been created in an irregular manner. Such entrances prove it difficult to recognize factors influencing their orientation and origin. Thus, many entrances have been created without a clear connection with the bedrock structure. Simultaneously, the entrance line is predominantly parallel to the MLE direction, which informs about the expected orientation of the inlets to the inner cave or cavity (Figure 11g).

The formation of single or two entrances to the cavity progresses from both the marginal and central parts of the forms, as in the case of gypsum tumuli landforms in the Sorbas region in Spain, where erosion is an important factor in broadening small inlets to the size of a large entrance [36,37].

4.7.5. Relation to Gypsum Tumuli

The origin of gypsum tumuli is not related to anhydrite dissolution and succeeding gypsum crystallization, but solely to the crystallization of secondary gypsum after gypsum dissolution within weathering gypsum rocks taking place in an arid or semi-arid climate or microclimate [36,37,108]. Morphologically, gypsum tumuli are generally domes similar to many anhydrite hydration landforms; however, they form tepee-shaped forms either, although much less frequently [37]. Researchers of gypsum tumuli in the Spanish region of Sorbas have recognized their maximum length up to 11.7 m [67], whereas in Sicily, up to 11 m [109] or 15 m [108], which is similar in value to the size of hydration forms. Similar to hydration landforms, the largest gypsum tumuli are less common. On the other hand, both hydration forms and gypsum tumuli have similar small dimensions in a plan view—a few tens of centimeters [37].

The significant morphometric difference between the hydration landforms and gypsum tumuli, as noted earlier [36,48], is a different height, determined as a maximum of 1.30 m for gypsum tumuli, which is significantly less than the 2.09 m recognized for the forms at Dingwall, ca. 3 m at Pisky [18,60] and 3 m for the Waldschmiede in Walkenried [4]. The difference between the maximum height of the tumuli and the hydration landforms is even larger, taking into account that the reported “height” of gypsum tumuli is not a real relative height but the distance measured from the bottom of the internal cavity to the top of the form [67]. The other morphometric difference is the higher convexity reached by hydration landforms, reflected by the ratio of elevation (relative height) to their lateral dimensions [36] (p. 927). There are also some differences in the shape of both forms related to different mechanisms of volume expansion and potentially higher volume increase and more complicated deformations in case of anhydrite hydration (resulting, e.g., in a higher steepness of side parts of the mature hydration forms such as Waldschmiede, the Great Tepee from Pisky, or some forms from Dingwall) [1,4] (Figure 6b,d in [9]) [18,49,61]. Some other structural differences between anhydrite hydration landforms and gypsum tumuli were noted by Calaforra and Pulido-Bosch [36].

4.7.6. Structural Characteristic

Stenson [48] recorded at Dingwall large hydration landforms (>2.0 m) with thicknesses of detached layer <10 cm and also small forms (<1.0 m) showing a thickness of >35 cm and concluded that the thickness depends neither on the size nor on the type (blister or tent) of hydration forms. Our data suggest, however, that the size of the forms depends to some extent on this thickness—the landforms larger in extent (longer) have a remarkably thicker detached rock layer (Figure 10d). The same rule was recognized very clearly in the gypsum tumuli [36,67]. The larger thickness of the detached layer may be related to deeper

localized hydration. Herrmann [45] believed that the greater the thickness of the detached layer, the greater the hydration cave.

The surface of hydration forms is commonly strongly fractured, and the majority of fractures are evidently the result of expansive anhydrite hydration. They formed during the growth of the landforms, when rock slabs rise up, deform, bend, break and push against each other. However, as proved above, some fractures have been evidently inherited from the joint system in the bedrock, occurring in the place where the hydration form is now. These joints commonly widened during the rise of the detached rock layer. The master joints significantly contribute to a greater density of fractures, recorded, e.g., in the EF (see Figure 12). It was demonstrated that with decreasing fracturing, the dimensions of forms increase, both in length and height (see Figure S3). This feature is related to the strength of the rock, which is significant when the rock is not fractured and weakens as soon as it is more fractured. The hydration forms densely covered with fractures, as rocks documented worldwide [110] are more prone to erosion and rapid transition into the destruction stage.

In addition, the density of fractures generally decreases when the thickness of the raised layer increases (Figure 14a), just as in the case of joints in sedimentary rocks, where the joint spacing increases with the rise in thickness of the rock layers [111,112]. In addition, contrary to Stenson's [48] opinion, fractures have been formed just as easily within both domed and tepee-shaped forms because both of them have a similar number of fractures (Figure 13).

4.8. Bedrock Structure Impact for Hydration Forms

Our observations suggest that the morphology of hydration forms at Dingwall is dependent on the structure of the anhydrite bedrock (Figure S9). In particular, the location of the entrances to the inner cavities and the way they have been opened are strongly dependent on the structural features of the rocks, such as master (and other) joints and layering. These features, the presence or absence of joints and layering, and surface fracture density appear to be the important factors controlling the development and structure of the hydration landforms at Dingwall. In general, three structural types of bedrocks can be distinguished, involving both master joints and pronounced layering, or one of them (Figure 15a–c).

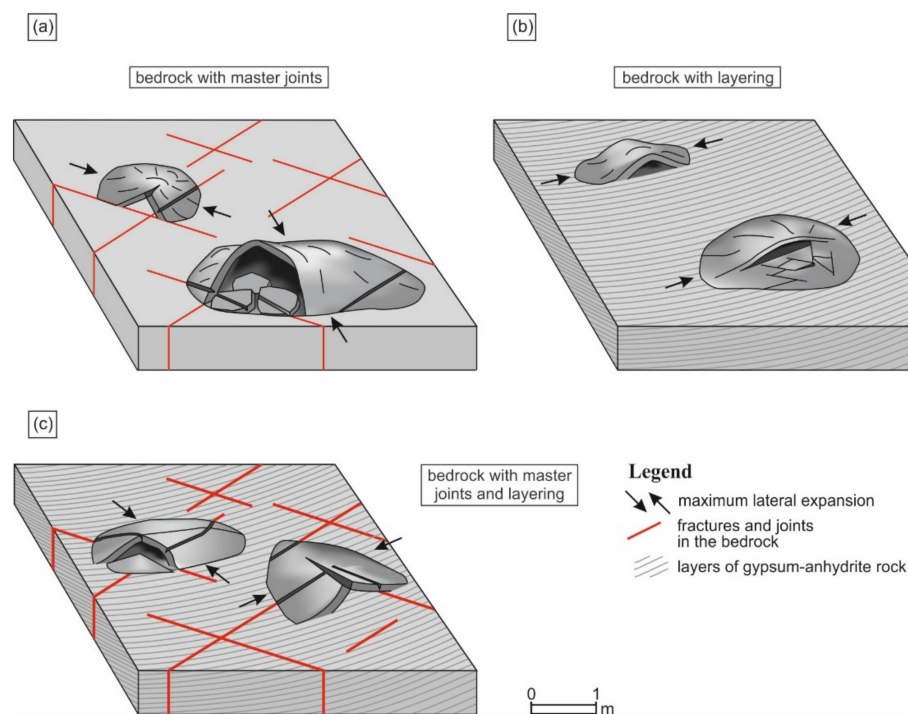


Figure 15. (a–c) Three structural types of bedrock influencing the development of hydration landforms. Note that the location of the entrances to hydration cavities and caves is determined by the presence of master joints and/or layering in the bedrock. Further explanations in the text.

4.8.1. Master Joints

These joints were present in the rock layer before they underwent detachment and uplift. The joints forming particular sets cross-cut, causing that the bottom of the quarry is usually divided into segments with triangular, rhombic or polygonal contours (e.g., Figure 11a) (Figure 1e in [14]). The presence of these blocks significantly influences the structure of the developing hydration landforms, fracture density and fracture orientations. Rock within the range of the form at the beginning of its uplift inherits older fractures or joints (Figure 3b). They affect its strength and cause distortions of the layer separated from the bedrock. Such distortions are mainly manifested by the collapse of fragments of the elevated rock, along with inherited fractures and the formation of entrances to the internal cavity. The collapse may occur along two fractures (joint sets) intersecting at a certain angle and creating segments (Figure 15a,c). Movements along the fracture surface may also lead to an uplift of the rock layer on one side of the fracture; on the other side, the rock may remain lower.

New fractures are also generated by expansive anhydrite hydration connected inter alia with the direction of MLE, affecting the development of landforms and their morphology (Figure 3b). These fractures—not related to earlier masters and other joints—are also the reason for weakening the strength of the rock layer. They equally favor the direction and location of rock detachment and uprising, and they are also a place for the formation of entrances to the inner cavity (Figures 11d and 15a).

4.8.2. Strike of Layers

Another impact on the morphology of hydration landforms is the strike of the rock layers. Observing its azimuth, it could be supposed that a similar orientation has some entrances to the internal cavities of the growing landforms (entrance lines; Figure 3) and also fractures within them. Moreover, in some cases, the orientation of the layers seems to control the azimuth of the elongation of the discussed forms. These observations lead to the conclusion that the strike of rock layers guides both the shape and orientation of the hydration landforms (direction of their elongation), as in the case of the site at the Alebastrovyje Islands [5], but in the study area that impact is less pronounced (Figure 15b).

4.8.3. Master Joints and Strike of Layers

The occurrence of both master joints and prominent layering in the bedrocks influences the development of hydration landforms even more (Figure 15c). The joints increase the fracture density, determine the structure of the growing form and affect the orientation of the entrance to the cavity. The strike of the layers can also influence the direction of elongation of the form. However, the influence of these factors is more complex and hardly predictable because it depends on the number of master joint sets (from 1 to 4), as well as the mutual orientation of joints and layering, which are changeable across the quarry.

5. Conclusions and Final Remarks

It was demonstrated that expansive hydration of anhydrite during the weathering of these rocks leads to the creation of peculiar convex landforms characterized by defined sizes and shapes. Such landforms studied in the abandoned gypsum quarry at Dingwall have developed for more than 65 years, counting since the time of anhydrite bedrock exposure, i.e., longer than the growth of hydration forms at the Pisky site and much shorter than at the Walkenried site, where the hydration continues for more than 300 years [52]. At present, the majority of the studied landforms (estimated at about 91%) seem to be in the mature or senile stage of development (Figure 2f). 62% of them have internal proper caves [96,97], being a unique speleological object known as hydration or swelling caves. Among them is one of the largest hydration caves, measuring $10.7 \times 6.6 \times 1.10$ m.

The landforms from Dingwall, similar to the other mentioned sites, are characterized by defined sizes and shapes. The two basic shapes include dome-like, dominating and tepee-like, less frequent; the latter is defined by a sharp crest. In a plan view, the landforms

vary from circular through oval to elongated in shape, with length (a) to width (b) ratio rarely exceeding 5:2 (Figure 6). These shapes are an idealized approximation of the real shapes, which are commonly irregular and complex and difficult to define and classify, particularly in the case of “senile” forms undergoing destruction.

The sizes of the studied landforms are limited. Most commonly, they are 1.8–8.0 m in length (90% of forms). The lower limit of length was not determined precisely, but presumably is a few tens of centimeters. The upper limit is 23 m, and as a rule, the longer the form, the less frequently it occurs. The relative height ranges from 0.33 to 2.09 m and is 0.83 m on average. The frequency distribution of sizes (length, width, relative height) confirms the general rule observed in the dimensions of many landforms characterized by “large numbers of small values and smaller numbers of large ones” [29] (p. 62). All of the obtained histograms appear to show right-skewed distributions, although the smallest sizes were not documented (Figure 6, Table 2).

The size of the hydration landforms depends mainly on the thickness of the detached rock layer—the thicker the layer, the larger the hydration form.

The length (a), width (b) and relative height (h_r) for the majority of forms overall show proportional relations, testifying that the hydration landforms preserve generally the same or very similar shape independent of their sizes. The relations between these basic parameters can be expressed by the following equations: $b = 0.67a$, $h_r = 0.16a$, $h_r = 0.23b$; with correlation (Pearson) coefficients (r) of 0.77, 0.75, and 0.63, respectively, indicating moderate correlation.

The convexity of hydration landforms was characterized by a b/h_r ratio—bulge degree. It ranges from 1.82 for the most convex forms to 8.58 for the least convex forms. According to the average value of this parameter, the domed forms are slightly less convex than the tepee-shaped ones.

Maximum lateral expansion, measured normally to the approximated crest line of the landforms, provides information on the strain responsible for the creation of their convex shape. Simplifying informs us about the direction of dominating “forces” pushing up or buckling the detached layer. Although MLE was most commonly normal or nearly normal to the elongation of the forms (46% of them), quite often, it was parallel to the elongation (29% of forms; Figure 7d,g). It can be concluded that the centers of accelerated greater volume expansion (crystallization of the secondary gypsum) were presumably located at sites near the erected forms, situated as a rule normally to their elongation or, less commonly, along this direction.

The development of hydration landforms depends on the structure of the bedrock on which they occur. The joint system present in the bedrock is inherited by the growing landforms—master joints are recognizable on almost half of the hydration forms. These earlier fractures determined the way of opening the entrance to the inner cavities or caves and weakened the stability of the lifted layers.

The layering in the massive bedrock without joints may control the orientation of both the landform elongation and the entrance to the internal cavity. The bedrock with both mentioned features has a more complex impact on the growing hydration forms, which depends on the mutual orientation of the layering and joints. Such landforms develop in a more complicated and unpredictable manner.

The number of fractures on the surface of hydration forms varies significantly. Both landforms without fractures and those with densely distributed fractures (with their total length up to 33.5 m per 10 m²) have been documented. Fractures are most common in the hydration forms developed on the bedrock disturbed by the extensive master joint system and are the least common in forms growing on the substrate without any visible joints or fractures.

Fractures on the landform surfaces are represented by the most common transverse, longitudinal and irregular ones, and the uncommon ones, such as spherical and radial. The durability of landforms over time depends on the number of fractures associated with them.

The authors hope that the presented geomorphometric documentation and characteristics of the hydration landforms will help in remote recognition of such forms and in distinguishing them from other similar objects, as well as in a better understanding of their not entirely clear origin.

The photogrammetric models and maps of the zone of the weathering anhydrite will help in monitoring, further analysis and study of the ongoing morphological evolution of the Dingwall quarry area.

In closing, it should be emphasized that expansive anhydrite hydration is still not a well-recognized process that requires further study. This process, which leads to swelling of the ground surface, can be very destructive. It currently takes place with highly catastrophic results in several urban and industrial areas around the world [14] (with references therein) [113–115]. In spite of many studies, engineering knowledge on how to prevent, control and stop this process is still insufficient. The Dingwall site is an excellent place where many aspects of the anhydrite hydration process can be directly investigated, and we hope that further research will contribute to addressing many of the unsolved anhydrite hydration problems.

Supplementary Materials: The following supporting information can be downloaded at: <https://www.mdpi.com/article/10.3390/app12157374/s1>, Table S1: Inventory of hydration landforms with basic morphometric parameters and GPS locations; Figure S1: Applied photogrammetric method—equipment, course of work and results; Figure S2: Hydration landforms on the orthophotomaps and digital surface models; Figure S3: Location of hydration landforms on the base map of satellite images with characteristics of their sizes; Figure S4: Location of hydration landforms with measured thickness of the detached layer on the base map of the satellite image; Figure S5: Frequency distribution diagrams of morphometric parameters characterizing hydration landforms; Figure S6: Dependence of relative height of hydration landforms on length, width, bulge degree and coefficient of circularity; Figure S7: Pattern of fractures within hydration forms; Figure S8: Traces of fractures and rock layers on the orthophotomaps of the quarry bottom; Figure S9: Exemplary hydration landforms influenced by structural type of bedrock.

Author Contributions: Conceptualization, A.J. and M.B.; methodology, A.J.; software, A.J.; validation, A.J. and M.B.; formal analysis, A.J.; investigation, A.J., F.V. and D.L.; resources, A.J.; data curation, A.J.; writing—original draft preparation, A.J. and M.B.; writing—review and editing, A.J. and M.B.; visualization, A.J.; supervision, M.B.; project administration, A.J.; funding acquisition, A.J. All authors have read and agreed to the published version of the manuscript.

Funding: This research was funded by the Ministry of Higher Education and Science project within the “Diamond Grant” program, grant no. 0002/DIA/2017/46.

Institutional Review Board Statement: Not applicable.

Informed Consent Statement: Not applicable.

Data Availability Statement: Not applicable.

Acknowledgments: The authors acknowledge the owner of the Dingwall quarry area, Gary Burchell for enabling the research work at the site, and Robert Ryan from the Nova Scotia Department of Energy and Mines for supplying the valuable geological information. Many thanks to Janet Connor and John Connor for providing the accommodation and support during expeditions to the Dingwall quarry. The authors also acknowledge Canada Transport for permission to launch the UAV in the quarry. The authors also thank the five reviewers and Editors of the volume for their contributions to improving the paper.

Conflicts of Interest: The authors declare no conflict of interest.

References

1. Reinboth, F. Die Waldschmiede bei Walkenried eingestützt. *Mitt. Verb. dt. Höhlen-u. Karstf.* **1967**, *13*, 68.
2. Reinboth, F. Die Zwerglöcher bei Walkenried am Südharz—Bemerkungen zur Frage der Quellungshöhlen. *Die Höhle Z. für Karst- und Höhlenkunde* **1997**, *48*, 1–13.
3. Hunt, C.O.; Gale, S.J.; Gilbertson, D.D. The UNESCO Libyan Valley Survey IX: Anhydrite and limestone karst of the Tripolitanian pre-desert. *Libyan Stud.* **1985**, *16*, 1–13. [[CrossRef](#)]
4. Reimann, M. Geologisch-lagerstättenkundliche und mineralogische Untersuchungen zur Vergipsung und Volumenzunahme der Anhydrite verschiedener geologischer Formationen unter natürlichen und labormäßigen Bedingungen. *Geol. Jahrb.* **1991**, *D97*, 21–125.
5. Yushkin, N.P. Supergeneration of Carboniferous anhydrites of Novaya Zemlya. *Polar. Geogr. Geol.* **1994**, *18*, 33–43. [[CrossRef](#)]
6. Reimann, M.; Vladi, F. Zur Entwicklung der sog. Zwergengirke am Sachsenstein bei Walkenried, Landkreis Osterode am Harz, Niedersachsen und vergleichende Beobachtungen zur rezenten Entstehung von Quellungshöhlen in einem aufgelassenen Gipssteinbruch bei Dingwall, Nova Scotia, Kanada. *Mitt. Verb. dt. Höhlen-u. Karstforscher* **2003**, *49*, 75–77.
7. Jarzyna, A.; Babel, M.; Ługowski, D.; Vladi, F.; Yatsyshyn, A.; Olszewska-Nejbert, D.; Nejbert, K.; Bogucki, A. Unique hydration caves and recommended photogrammetric methods for their documentation. *Geoheritage* **2020**, *12*, 27. [[CrossRef](#)]
8. Vladi, F.; Babel, M. Recent growth and decay of the hydration (swelling) caves in the former gypsum quarry of Dingwall in Cape Breton, Nova Scotia, Canada. In *The Weathering of Anhydrite and Gypsum Rocks*; Babel, M., Olszewska-Nejbert, D., Nejbert, K., Eds.; GIMPO Agencja Wydawniczo-Poligraficzna: Warsaw, Poland, 2020; pp. 223–232. [[CrossRef](#)]
9. Vladi, F.; Babel, M.; Jarzyna, A. Wachstum und Zerfall rezenter Quellungshöhlen im ehemaligen Gipssteinbruch von Dingwall in Cape Breton, Nova Scotia, Kanada, nebst Anmerkungen zum dortigen Sulfatkarst und dem Forschungsstand. *Abh. Zur Karst- und Höhlenkunde* **2022**, *40*, 119–134.
10. Mossop, G.D.; Shearman, D.J. Origin of secondary gypsum rocks. *Trans. Inst. Min. Metall. Sec. B Appl. Earth Sci.* **1973**, *82*, B147–B154.
11. Zanbak, C.; Arthur, R.C. Geochemical and engineering aspects of anhydrite/gypsum phase transition. *Bull. Assoc. Eng. Geol.* **1986**, *23*, 419–433. [[CrossRef](#)]
12. James, A.N. *Soluble Materials in Civil Engineering*; Ellis Horwood: New York, NY, USA, 1992; pp. 1–434.
13. Babel, M.; Olszewska-Nejbert, D.; Ługowski, D.; Nejbert, K.; Jacyszyn, A. Petrogenesis of the zone of present day anhydrite weathering at Pisky near Lviv. In *The Weathering of Anhydrite and Gypsum Rocks*; Babel, M., Olszewska-Nejbert, D., Nejbert, K., Eds.; GIMPO Agencja Wydawniczo-Poligraficzna: Warsaw, Poland, 2020; pp. 145–213. (In Polish with English Summary) [[CrossRef](#)]
14. Jarzyna, A.; Babel, M.; Ługowski, D.; Vladi, F. Petrographic record and conditions of expansive hydration of anhydrite in the recent weathering zone at the abandoned Dingwall gypsum quarry, Nova Scotia, Canada. *Minerals* **2022**, *12*, 58. [[CrossRef](#)]
15. Biese, W. Über Höhlenbildung, Teil 1. Entstehung der Gipshöhlen am südlichen Harzrand und am Kyffhäuser. *Abh. Preußischen Geol. Landesanst. Neue Folge* **1931**, *137*, 1–71.
16. Myers, A.J. Geology of the Alabaster Cavern area. In *Guide to Alabaster Cavern and Woodward County, Oklahoma*; Guidebook 15; Myers, A.J., Gibson, A.M., Glass, B.P., Patrick, C.R., Eds.; Oklahoma Geological Survey: Norman, OK, USA, 1969; pp. 6–16.
17. Breisch, R.L.; Wefer, F.L. The shape of gypsum bubbles. In *Proceedings of the 8th International Congress of Speleology*; Beck, B.F., Ed.; National Speleological Society: Huntsville, AL, USA, 1981; Volume 2, pp. 757–759.
18. Jarzyna, A.; Ługowski, D.; Olszewska-Nejbert, D.; Jacyszyn, A.; Babel, M. Inventory of the dome-shaped hydration landforms from the area of weathering anhydrite rocks at Pisky near Lviv. In *The Weathering of Anhydrite and Gypsum Rocks*; Babel, M., Olszewska-Nejbert, D., Nejbert, K., Eds.; GIMPO Agencja Wydawniczo-Poligraficzna: Warsaw, Poland, 2020; pp. 47–77. (In Polish with English Summary) [[CrossRef](#)]
19. Tsui, P.C.; Cruden, D.M. Deformation associated with gypsum karst in the Salt River Escarpment, northeastern Alberta. *Can. J. Earth Sci.* **1984**, *21*, 949–959. [[CrossRef](#)]
20. Babel, M.; Yatsyshyn, A.; Ługowski, D.; Nejbert, K.; Olszewska-Nejbert, D.; Bogucki, A.; Kremer, B. Swelling caves from the weathering zone of anhydrite rocks in western Ukraine. In *Sedimentology at the Crossroads of New Frontiers, Proceedings of the 19th International Sedimentological Congress, Geneva, Switzerland, 18–22 August 2014, Abstracts Book*; Université de Genève: Geneva, Switzerland, 2014; p. 35.
21. Kraus, E.H. Hydration caves. *Sci. New Ser.* **1905**, *22*, 502–503.
22. Gorbunova, K.A. Caves of hydration. *Peshchery* **1978**, *17*, 61–63. (In Russian)
23. Bögli, A. *Karst Hydrology and Physical Speleology*; German Edition, Karsthydrographie und Physische Speläologie, 1978; Schmid, J.C., Translator; Springer: Berlin, Germany, 1980; pp. 1–270. [[CrossRef](#)]
24. Kempe, S. Gypsum karst of Germany. *Int. J. Speleol.* **1996**, *25*, 209–224. [[CrossRef](#)]
25. Bella, P. *Genetické Typy Jaskýň*; Speleologia Slovaca 2; Verbum: Ružomberok, Slovakia, 2011; pp. 1–220. (In Slovak with English Summary)
26. Bella, P.; Gaál, L. Genetic types of non-solution caves. In *Proceedings of the 16th International Congress of Speleology, Brno, Czech Republic, 21–28 July 2013*; Filippi, M., Bosák, P., Eds.; Speleological Society: Praha, Czech Republic, 2013; Volume 3, pp. 237–242.

27. White, W.B.; Culver, D.C. Cave, definition of. In *Encyclopedia of Caves*, 3rd ed.; White, W.B., Culver, D.C., Pipan, T., Eds.; Elsevier: Amsterdam, The Netherlands, 2019; pp. 255–259. [CrossRef]
28. Ługowski, D.; Babel, M. Distribution of gypsum content in anhydrite hydration dome from Pisky near Lviv and its development. In *The Weathering of Anhydrite and Gypsum Rocks*; Babel, M., Olszewska-Nejbert, D., Nejbert, K., Eds.; GIMPO Agencja Wydawniczo-Poligraficzna: Warsaw, Poland, 2020; pp. 135–144, (In Polish with English Summary). [CrossRef]
29. Evans, I.S. Scale-specific landforms and aspects of the land surface. In *Concepts and Modelling in Geomorphology: International Perspectives*; Evans, I.S., Dikau, R., Tokunaga, E., Ohmori, H., Hirano, M., Eds.; TERRAPUB: Tokyo, Japan, 2003; pp. 61–84.
30. MacMillan, R.A.; Shary, P.A. Landforms and landform elements in geomorphometry. *Dev. Soil Sci.* **2009**, *33*, 227–254. [CrossRef]
31. Mokarram, M.; Sathyamoorthy, D. A review of landform classification methods. *Spat. Inf. Res.* **2018**, *26*, 647–660. [CrossRef]
32. Mark, D.M. Geomorphometric parameters: A review and evaluation. *Geogr. Ann.* **1975**, *57*, 165–177. [CrossRef]
33. Pike, R.J. Geomorphometry—Diversity in quantitative surface analysis. *Prog. Phys. Geogr.* **2000**, *24*, 1–20. [CrossRef]
34. Pike, R.J.; Evans, I.; Hengl, T. Geomorphometry: A brief guide. *Dev. Soil Sci.* **2009**, *33*, 227–254. [CrossRef]
35. Muzirafuti, A.; Boualoul, M.; Barreca, G.; Allaoui, A.; Bouikbane, H.; Lanza, S.; Crupi, A.; Randazzo, G. Fusion of remote sensing and applied geophysics for sinkholes identification in Tabular Middle Atlas of Morocco (the Cause of El Hajeb): Impact on the protection of water resource. *Resources* **2020**, *9*, 51. [CrossRef]
36. Calaforra, J.M.; Pulido-Bosch, A. Genesis and evolution of gypsum tumuli. *Earth Surf. Proc. Land.* **1999**, *24*, 919–930. [CrossRef]
37. Jarzyna, A.; Babel, M.; Ługowski, D. Morphological diversity and form evolution of the gypsum tumuli from Sorbas region in Spain. In *The Weathering of Anhydrite and Gypsum Rocks*; Babel, M., Olszewska-Nejbert, D., Nejbert, K., Eds.; GIMPO Agencja Wydawniczo-Poligraficzna: Warsaw, Poland, 2020; pp. 233–269, (In Polish with English Summary). [CrossRef]
38. Gutiérrez, F.; Gutiérrez, M. *Landforms of the Earth: An Illustrated Guide*; Springer: Berlin/Heidelberg, Germany, 2016; pp. 1–270. [CrossRef]
39. Breisch, R.L. The truth about gypsum caves. *Natl. Speleol. Soc. News* **1978**, *36*, 183–185.
40. Kraus, E.H. On the origin of the caves of the island of Put-in-Bay, Lake Erie. *Am. Geol.* **1905**, *35*, 167–171.
41. Cottingham, K. The origin of the caves at Put-in-Bay, Ohio. *Ohio J. Sci.* **1919**, *20*, 38–42.
42. Muir, J.L. Anhydrite–gypsum problem of Blaine Formation, Oklahoma. *Am. Assoc. Petr. Geol. B.* **1934**, *18*, 1310–1311, The text discussion by Griley. [CrossRef]
43. Verber, J.L.; Stansbury, D.H. Caves in Lake Erie Islands. *Ohio J. Sci.* **1953**, *53*, 358–362.
44. Kes, A.S. Gypsum domes in a desert. *Priroda* **1961**, *2*, 114–115. (In Russian)
45. Herrmann, A. Vergipsung und oberflächenformung im gipskarst. In *Proceedings of the Third International Congress of Speleology, Vienna, Austria, 1963*; Trimmel, H., Ed.; Verband Österreichischer Höhlenforscher: Vienna, Austria, 1966; Volume 5, pp. 99–108. Available online: http://uis-speleo.org/wp-content/uploads/2020/07/3rd_Kongress_fuer_Spelaeologie_Band_V.pdf (accessed on 13 July 2022).
46. Gorbunova, K.A. Exogenetic karst tectonics. In *Proceedings of the 7th International Speleological Congress, Sheffield, 1977*; Ford, T.D., Ed.; BCRA: Bridgwater, UK, 1977; pp. 222–223. Available online: <http://uis-speleo.org/wp-content/uploads/2020/08/Proceedings-of-The-7th-International-Speleological-Congress-Sheffield-England-September-1977.pdf> (accessed on 13 July 2022).
47. Völker, C.; Völker, R. Gipskuppen und Gipsbuckel—Elemente der Sulfatkarstlandschaft. *Mitt. Karstmus. Heimkehle* **1988**, *19*, 1–19.
48. Stenson, R.E. The Morphometry and Spatial Distribution of Surface Depressions in Gypsum, with Examples from Nova Scotia, Newfoundland and Manitoba. Master’s Thesis, McMaster University, Hamilton, ON, Canada, 1990; pp. 1–134.
49. Reimann, M. Quellungshöhlen am südharz, landschaftsprägende auswirkung der vergipsung von anhydritstein. In *Proceedings of the Zechstein 1987—International Symposium—Abstracts, Posters, Program, Kassel, Hannover, Germany, 28 April–9 May 1987*; Bernd, K., Schröder, B., Eds.; Poster, MS of the Summary. p. 9.
50. Stafford, K.W.; Ehrhart, J.; Majzoub, A.; Shields, J.; Brown, W. Unconfined hypogene evaporite karst: West Texas and southeastern New Mexico, USA. *Int. J. Speleol.* **2018**, *47*, 293–305. [CrossRef]
51. Beyrich, E. *Erläuterungen zur Geologischen Spezialkarte von Preussen und den Thüringischen Staaten*; No. 255, Blatt Ehrlich, Bande 6, Blatt 2; Verlag von J.H. Neumann: Berlin, Germany, 1870; pp. 1–18.
52. Behrens, G.H. *Hercynia Curiosa Oder Curiöser Hartz-Wald*; Verlegt Carl Chriftian Neuenhahn: Nordhausen, Germany, 1703; pp. 1–216. Available online: http://www.deutschestextarchiv.de/book/show/behrens_hercynia_1703 (accessed on 6 May 2022).
53. Stolberg, F. *Die Höhlen des Harzes, Bd. 1. Einleitung und Südharzer Zechsteinhöhlen. Sonderausgabe der illustrierten Monatsschrift "Der Harz", Heft 2*; Eilers-Verlag G.m.b.H.: Magdeburg, Germany, 1926; pp. 1–40.
54. Babel, M.; Jacyszyn, A.; Olszewska-Nejbert, D.; Nejbert, K.; Bogucki, A.; Maksymiów, I.; Mik, W.; Bermes, A.; Ługowski, D.; Kacprzak, K.; et al. Jaskinie z pęcznienia (ang. swelling caves) w strefie współczesnego wietrzenia anhydrytów w kamieniołomie Pisky w okolicach Lwowa. In *Od Czarnohory po Góry Świętokrzyskie—Geologiczne Peregrynacje, Polsko-Ukraińska Sesja Naukowa, Warszawa, Bocheniec, 15–19 Października 2013*; Babel, M., Dzierżek, J., Olszewska-Nejbert, D., Eds.; Instytut Geologii Podstawowej WG UW: Warsaw, Poland, 2013; pp. 19–26. [CrossRef]

55. Babel, M.; Yatsyshyn, A.; Bogucki, A.; Jarzyna, A.; Ługowski, D.; Olszewska-Nejbert, D.; Nejbert, K.; Kotowski, J.; Przybylik, G.; Bermes, A.; et al. Development of the unique landforms in the zone of weathering gypsum-anhydrite rocks at Pisky (Shchyrka river valley, Dniester basin). In *Scientific Principles of Conservation Management of Ecosystems in the Dniester Canyon Area, Proceedings of the Second International Scientific and Practical Conference Dedicated to the 170th Anniversary of Publication of Rudolf Kner's Work Which Marked the Beginning of the Profound Paleontological Investigations in the Dniester Canyon, Zalishchyky, Ternopil, Ukraine, 14–15 September 2017*; Skilsky, I.V., Vikyrchak, O.K., Eds.; Druk Art: Chernivtsi, Ukraine, 2017; pp. 23–25. [[CrossRef](#)]
56. Ługowski, D.; Jarzyna, A. The map of the site of weathering anhydrites and hydration caves at Pisky at environs of Lviv. In *The Weathering of Anhydrite and Gypsum Rocks*; Babel, M., Olszewska-Nejbert, D., Nejbert, K., Eds.; GIMPO Agencja Wydawniczo-Poligraficzna: Warsaw, Poland, 2020; pp. 21–48. (In Polish with English Summary) [[CrossRef](#)]
57. Jarzyna, A. Geological Setting and Morphology of the Site of the Weathering Miocene Anhydrites at Pisky near Lviv. Master's Thesis, University of Warsaw, Warsaw, Poland, 2021; pp. 1–131. (In Polish with English Summary)
58. Babel, M.; Bogucki, A.; Jacyszyn, A.; Ługowski, D.; Olszewska-Nejbert, D.; Nejbert, K.; Jarzyna, A.; Bermes, A.; Przybylik, G.; Tomeniuk, O. Weathering anhydrites at Pisky quarry, Part I. General characteristic. In *Weathering of Gypsum and Anhydrite Rocks, Proceedings of the Polish-Ukrainian Scientific Seminar, Warsaw, Poland, 19–21 January 2017*; Babel, M., Olszewska-Nejbert, D., Nejbert, K., Eds.; IGP WG UW: Warszawa, Poland, 2017; pp. 18–22. (In Polish) [[CrossRef](#)]
59. Maksymiuk, I.P. Geomorphological Effects of the Hydration Processes in the Gypsum Layer of the "Pisky" Section. Master's Thesis, Faculty of Geography, University of Lviv, Lviv, Ukraine, 2013; pp. 1–70. (In Ukrainian)
60. Ługowski, D.; Jarzyna, A.; Babel, M.; Nejbert, K. Data collecting methods used in the field study of weathering anhydrites at Pisky near Lviv. *Biul. Państwowego Inst. Geol.* **2016**, *466*, 201–214. [[CrossRef](#)]
61. Jarzyna, A.; Babel, M.; Ługowski, D.; Vladi, F. Preliminary morphological analysis of the anhydrite hydration forms at Dingwall (Canada, Nova Scotia) on the base of photogrammetric documentation. In *Forum GIS UW. GIS na Uniwersytecie Warszawskim. Materiały Pokonferencyjne z 5. i 6. Forum GIS na UW*; Chyla, J., Lechnio, J., Stepień, M., Zaszewski, D., Eds.; UW WG, WGiSR, IAWH: Warsaw, Poland, 2019; pp. 92–102. (In Polish with English Summary) [[CrossRef](#)]
62. Twidale, C.R.; Bourne, J.A. On the origin of A-tents (pop-ups), sheet structures, and associated forms. *Prog. Phys. Geogr.* **2009**, *33*, 147–162. [[CrossRef](#)]
63. Demicco, R.V.; Hardie, L.A. *Sedimentary Structures and Early Diagenetic Features of Shallow Marine Carbonate Deposits*; SEPM Atlas Series; SEPM: Tulsa, OK, USA, 1994; pp. 1–255. [[CrossRef](#)]
64. Jennings, J.N.; Twidale, C.R. Origin and implications of the A-tent, a minor granite landform. *Aust. Geogr. Stud.* **1971**, *9*, 41–53. [[CrossRef](#)]
65. Folk, R.L.; Begle Patton, E. Buttressed expansion of granite and development of grus in Central Texas. *Z. Geomorphol. Neue Folge* **1982**, *26*, 17–32.
66. Ericson, K.; Olvmo, M. A-tents in the Central Sierra Nevada, California: A geomorphological indicator of tectonic stress. *Phys. Geogr.* **2004**, *25*, 291–312. [[CrossRef](#)]
67. Pulido-Bosch, A. Le karst dans le gypses de Sorbas (Almeria). Aspects morphologiques et hydrogéologiques. In *Karst et Cavités d'Andalousie, Cordillères Bétiqes Centrales et Occidentales*; Karstologia, Mémoires, 1; Association Française de Karstologie: Nîmes, France, 1986; pp. 27–35.
68. Von Gaertner, H.-R. Petrographie und paläogeographische Stellung der Gipse vom Südrande des Harzes. *Jahrb. Preußischen Geol. Landesanst. Berl.* **1933**, *53*, 655–694.
69. Hargitai, H.; Kereszturi, A. *Encyclopedia of Planetary Landforms*; Springer: New York, NY, USA, 2015; pp. 1–2460. [[CrossRef](#)]
70. Bishop, J.L.; Yeşilbaş, M.; Hinman, N.W.; Burton, Z.F.M.; Englert, P.A.J.; Toner, J.D.; McEwen, A.S.; Gulick, V.C.; Gibson, E.K.; Koeberl, C. Martian subsurface cryosalt expansion and collapse as trigger for landslides. *Sci. Adv.* **2021**, *7*, eabe4459. [[CrossRef](#)]
71. Neale, E.R.W. *Geology, Dingwall, Nova Scotia, Map 1124A*; Geological Survey of Canada, Department of Mines and Technical Surveys: Ottawa, ON, Canada, 1963.
72. Adams, G.C. Gypsum and anhydrite resources in Nova Scotia. *Econ. Geol. Ser.* **1991**, *91*, 1–293.
73. Wiebe, R.A. Igneous and tectonic events in northeastern Cape Breton Island, Nova Scotia. *Can. J. Earth Sci.* **1972**, *9*, 1262–1277. [[CrossRef](#)]
74. Lynch, G.; Tremblay, C. Late Devonian–Carboniferous detachment faulting and extensional tectonics in western Cape Breton Island, Nova Scotia, Canada. *Tectonophysics* **1994**, *238*, 55–69. [[CrossRef](#)]
75. Grant, D.R. Quaternary geology, Cape Breton Island, Nova Scotia. *Geol. Surv. Can.* **1994**, *482*, 1–159. [[CrossRef](#)]
76. Moseley, M. Genesis of schlottenkarren on the Avon Peninsula of Nova Scotia (Canada) with implications for the geochronology of evaporate karsts and caves of Atlantic Canada. *Int. J. Speleol.* **2017**, *46*, 267–276. [[CrossRef](#)]
77. Ford, D. Principal features of evaporite karst in Canada. *Carbonate Evaporite* **1997**, *12*, 15–23. [[CrossRef](#)]
78. Stenson, R.E.; Ford, D.C. Rillenkarren on gypsum in Nova Scotia. *Geogr. Phys. Quatern.* **1993**, *47*, 239–243. [[CrossRef](#)]
79. Climate-Data.org. Available online: <https://en.climate-data.org/north-america/canada/nova-scotia/dalem-lake-98946/> (accessed on 18 September 2021).
80. Zepner, L.; Karrasch, P.; Wiemann, F.; Bernard, L. ClimateCharts.net—An interactive climate analysis web platform. *Int. J. Digit. Earth* **2021**, *14*, 338–356. [[CrossRef](#)]

81. Clark, C.D.; Hughes, A.L.C.; Greenwood, S.L.; Spagnolo, M.; Ng, F.S.L. Size and shape characteristics of drumlins, derived from a large sample, and associated scaling laws. *Quatern. Sci. Rev.* **2009**, *28*, 677–692. [CrossRef]
82. Spagnolo, M.; Clark, C.D.; Hughes, A.L.C.; Dunlop, P.; Stokes, C.R. The planar shape of drumlins. *Sediment. Geol.* **2010**, *232*, 119–129. [CrossRef]
83. Maclachlan, J.C.; Eyles, C.H. Quantitative geomorphological analysis of drumlins in the Peterborough Drumlin Field, Ontario, Canada. *Geogr. Ann. Ser. A Phys. Geogr.* **2013**, *95*, 125–144. [CrossRef]
84. Spagnolo, M.; Clark, C.D.; Hughes, A.L.C. Drumlin relief. *Geomorphology* **2012**, *153–154*, 179–191. [CrossRef]
85. Dadlez, R.; Jaroszewski, W. *Tektonika*; Wydawnictwo Naukowe PWN: Warsaw, Poland, 1994; pp. 1–743.
86. Mathumaniraja, C.K.; Anbazhagan, S.; Jothibas, A.; Chinnamuthu, M. Remote sensing and fuzzy logic approach for artificial recharge studies in hard rock terrain of South India. In *GIS and Geostatistical Techniques for Groundwater Science*; Senapathi, V., Viswanathan, P.M., Chung, S.Y., Eds.; Elsevier: Amsterdam, The Netherlands, 2019; pp. 91–112. [CrossRef]
87. Triggs, B.; Mclauchlan, P.; Hartley, R.; Fitzgibbon, A. Bundle adjustment—A modern synthesis. In *Vision Algorithms: Theory and Practice*; IWVA 1999, Lecture Notes in Computer Science; Triggs, B., Zisserman, A., Szeliski, R., Eds.; Springer: Berlin/Heidelberg, Germany, 2000; Volume 1883, pp. 1–71. [CrossRef]
88. Snavey, K.N. Scene Reconstruction and Visualization from Internet Photo Collections. Ph.D. Thesis, University of Washington, Seattle, WA, USA, 2008; pp. 1–192.
89. Westoby, M.J.; Brasington, J.; Glasser, N.F.; Hambrey, M.J.; Reynolds, J.M. ‘Structure-from-motion’ photogrammetry: A low-cost, effective tool for geoscience applications. *Geomorphology* **2012**, *179*, 300–314. [CrossRef]
90. Agisoft. *Agisoft PhotoScan User Manual Professional Edition, Version 1.2*; Agisoft LLC: St. Petersburg, Russia, 2016; pp. 1–97.
91. Randazzo, G.; Italiano, F.; Micallef, A.; Tomasello, A.; Cassetti, F.P.; Zammit, A.; D’Amico, S.; Saliba, O.; Cascio, M.; Cavallaro, F.; et al. WebGIS Implementation for dynamic mapping and visualization of coastal geospatial data: A case study of BESS project. *Appl. Sci.* **2021**, *11*, 8233. [CrossRef]
92. Rose, J.; Letzer, J.M. Drumlin measurements: A test of the reliability of data derived from 1:25,000 scale topographic maps. *Geol. Mag.* **1975**, *112*, 361–371. [CrossRef]
93. Turner, K. What’s the Difference among 2-D, 2.5-D, 3-D and 4-D? Applied Geoscience Forum, GIS World Article. 1997. Available online: http://dusk.geo.orst.edu/gis/gis_world_article.pdf (accessed on 13 July 2022).
94. Price, M.H. *Mastering ArcGIS*, 7th ed.; McGraw-Hill Education: New York, NY, USA, 2016; pp. 1–606.
95. Devore, J.L. *Probability and Statistics for Engineering and the Sciences*, 9th ed.; Cengage Learning: Boston, MA, USA, 2016; pp. 1–715.
96. Curl, R.L. On the definition of a cave. *NSS Bull.* **1964**, *26*, 1–6.
97. Curl, R.L. Entranceless and fractal caves revisited. In *Karst Modeling, Proceedings of the Symposium, Charlottesville, VA, USA, 24–27 February 1999*; Karst Waters Institute Special Publication 5; Palmer, A.N., Palmer, M.V., Sasowsky, I.D., Eds.; Karst Waters Institute Inc.: Charles Town, WV, USA, 1999; pp. 183–185.
98. Twiss, R.J.; Moores, E.M. *Structural Geology*, 2nd ed.; W.H. Freeman and Company: New York, NY, USA, 2007; pp. 1–736. [CrossRef]
99. Potter, P.E.; Pettijohn, F.J. *Paleocurrents and Basin Analysis*, 2nd ed.; Springer: Berlin/Heidelberg, Germany, 1977; pp. 1–425. [CrossRef]
100. Peacock, D.C.P.; Sanderson, D.J.; Rotevatn, A. Relationship between fractures. *J. Struct. Geol.* **2017**, *106*, 41–53. [CrossRef]
101. Hancock, P.L. Brittle microtectonics: Principles and practice. *J. Struct. Geol.* **1985**, *7*, 437–457. [CrossRef]
102. Laslett, G.M. Censoring and edge effects in areal and line transect sampling of rock joint traces. *Math. Geol.* **1982**, *14*, 125–140. [CrossRef]
103. Hydration Caves. Available online: <http://hydrationcaves.com/en/77-hydration-forms/> (accessed on 8 May 2022).
104. Beales, F.W.; Oldershaw, A.E. Evaporite-solution brecciation and Devonian carbonate reservoir porosity in Western Canada. *Am. Assoc. Petr. Geol. B.* **1969**, *53*, 503–512. [CrossRef]
105. Curl, R.L. Caves as a measure of karst. *J. Geol.* **1966**, *74*, 798–830. [CrossRef]
106. Webb, T.C. Geology and economic development of early Carboniferous marine evaporates, southeastern New Brunswick. In *Lands, Minerals and Petroleum Division; Field Guide No. 6*; Lands, Minerals and Petroleum Division, Department of Natural Resources: Tracadie-Sheila, NB, Canada, 2010; pp. 1–71.
107. Ball, P. *The Self-Made Tapestry: Pattern Formation in Nature*; Oxford University Press: Oxford, UK, 2001; pp. 1–312.
108. Ferrarese, F.; Macaluso, T.; Madonia, G.; Palmeri, A.; Sauro, U. Solution and recrystallisation processes and associated landforms in gypsum outcrops of Sicily. *Geomorphology* **2002**, *49*, 25–43. [CrossRef]
109. Macaluso, T.; Sauro, U. Aspects of weathering and landforms evolution on gypsum slopes and ridges of Sicily. *Suppl. Geogr. Fis. Dinam. Quat.* **1998**, *3*, 91–99.
110. Scott, D.N.; Wohl, E.E. Bedrock fracture influence on geomorphic process and form across process domains and scales. *Earth Surf. Proc. Land.* **2018**, *44*, 27–45. [CrossRef]
111. Narr, W.; Suppe, J. Joint spacing in sedimentary rocks. *J. Struct. Geol.* **1991**, *13*, 1037–1048. [CrossRef]
112. Shaocheng, J.; Zheming, Z.; Zichao, W. Relationship between joint spacing and bed thickness in sedimentary rocks: Effects of interbed slip. *Geol. Mag.* **1998**, *135*, 637–655. [CrossRef]
113. Butscher, C.; Mutschler, T.; Blum, P. Swelling of clay-sulfate rocks: A review of processes and controls. *Rock Mech. Rock Eng.* **2016**, *49*, 1533–1549. [CrossRef]

-
114. Fleuchaus, P.; Blum, P. Damage event analysis of vertical ground source heat pump systems in Germany. *Geotherm. Energy* **2017**, *5*, 1–15. [[CrossRef](#)]
 115. Hou, Z.; Wu, J. A practical swelling constitutive model of anhydrite and its application on tunnel engineering. *Res. Sq.* **2022**. [[CrossRef](#)]